CASL-U-2015-0143-000

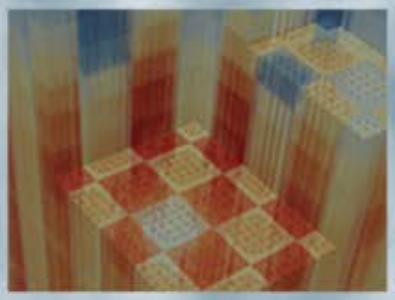

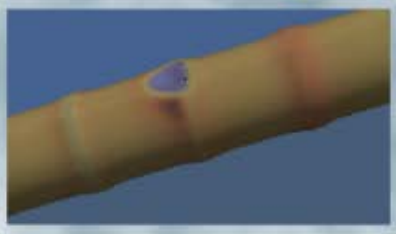

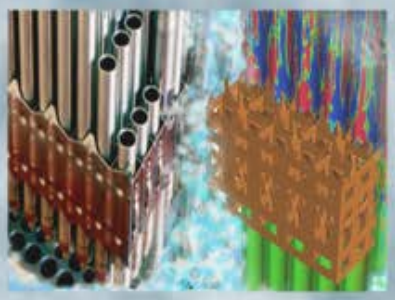

Babcock & Wilcox Critical Experiment Calculations to Support MPACT Verification

J. A. Kulesza, University of Michigan
S. G. Stimpson, Oak Ridge National Laboratory
A. R. Gerlach, University of Michigan
D. R. Jabaay, University of Michigan

April 24, 2015

REVISION LOG

Revision	Date	Affected Pages	Revision Description
0		All	Initial Release

Document pages that are:

Export Controlled _____None_____

IP/Proprietary/NDA Controlled_____None_____

Sensitive Controlled_____None_____

Requested Distribution:

To:

Copy:

EXECUTIVE SUMMARY

This report describes a series of benchmark calculations performed using the method of characteristics radiation transport code MPACT to verify its radial transport and axial buckling calculation capabilities. The benchmarks are based on a series of Babcock & Wilcox critical assembly configurations analyzed in what are commonly known as the B&W-1484 benchmark experiment and the B&W-1810 benchmark experiment.

The B&W-1484 experiment consists of 21 critical configurations (identified herein as 4:1 – 4:21) that simulated a variety of close-packed light water reactor (LWR) fuel storage configurations. Criticality measurements were performed and a series of Monte Carlo criticality calculations were also performed at the time to create an analytical basis for comparison with the experimental data.

Later, the B&W-1810 experiment consisted of 23 critical core configurations (identified herein as 8:1 – 8:23) to assess the effect of gadolinium (Gd_2O_3) absorbers used to permit higher than then-traditional assembly burnups and was designed to also be usable as a future benchmark.

Some of the critical experiment configurations are more relevant than others to the verification of MPACT. Therefore, only a subset of the available 44 core configurations were examined in-depth; those cores were: 4:1 – 4:3 and 8:1 – 8:10 and 8:12 – 8:17. The necessary inputs were prepared for Cores 4:4 – 4:21; however, they were not analyzed herein. In addition, the 3D KENO models for Cores 4:1 and 4:2 were updated and re-executed and then collapsed to 2D and executed to provide an additional form of cross-verification.

In summary, the results for MPACT are reasonable but there is room for improvement in terms of both effective eigenvalue as well as the fission rate distributions calculated. For the B&W-1484 cases, agreement was within 200 pcm of the measured eigenvalue for cases using P_2 scattering. Those cases using a NLC and P_1-outscatter transport-corrected P_0 (TCP_0) scattering method exhibited flux negativity enroute to the converged solution (with P_1-outscatter resulting in some converged negative fluxes). As an attempted fix-up, the TCP_0 (NLC) cases had all negative cross sections in groups corresponding to energies greater than 1 MeV truncated to zero (i.e., Limited TCP_0). For the various Core 4:3 subcases this fix-up was a benefit (resulting in eigenvalues within 100 pcm of the expected value); however, due to the disparate behavior of Cores 4:1 and 4:2 no significant benefit was observed. For the B&W-1810 cases, agreement was generally within 50-100 pcm of critical for those cases using P_2 scattering and 150-250 pcm for cases using NLC TCP_0 scattering. For the fission rate distributions, the root-mean-squared value was 77 pcm for and 208 pcm for P_2 and TCP_0 scattering, respectively, with a maximum discrepancy of 112 pcm and 261 pcm for P_2 and TCP_0 scattering, respectively.

Future work includes additional investigation into the flux negativity behavior witnessed and pursuing a transport-correction method that does not induce flux negativity at any point. It is also recommended that a rigorous method to calculate buckling on a case-by-case basis be developed and implemented to supplant the use of historical values.

CONTENTS

FIGURES

TABLES

ACRONYMS

AMA	Advanced Modeling Applications
ATWS-ED	Anticipated Transient without Scram – Emergency Depressurization
BDM	boron deposition model
BWR	boiling water reactor
CASL	Consortium for Advanced Simulation of Light Water Reactors
CHF	Critical Heat Flux
CILC	CRUD-induced localized corrosion
CIPS	CRUD-induced power shift
CFD	computational fluid dynamics
CP	Challenge Problem
CRUD	corrosion-related unidentified deposits or Chalk River unidentified deposits
CTF	COBRA-TF subchannel thermal-hydraulics code
CZP	Cold Zero Power
DA	data assimilation
DBA	design basis accident
DNB	departure from nucleate boiling
DOE	US Department of Energy
DOE NE	US Department of Energy Office of Nuclear Energy
DOE NR	US Department of Energy Office of Naval Reactors
DTK	Data Transfer Kit
DVE	Digital Video Enterprises
EIH	Energy Innovation Hub
ELT	Extended Leadership Team
EOI	expression of interest
EPRI	Electric Power Research Institute
FA	Focus Area
FAD	fuel assembly distortion
FMC	Fuel Materials and Chemistry
FOA	Funding Opportunity Announcement
FSI	fluid-structure interaction
GTRF	grid-to-rod-fretting
HFP	Hot Full Power
HPC	high-performance computing
HZP	Hot Zero Power
IC	Industry Council
INCITE	innovative and novel computational impact on theory and experiment
INL	Idaho National Laboratory
IP	intellectual property
iPWR	integral PWR
ISV	independent software vendor
LANL	Los Alamos National Laboratory
LOCA	loss of coolant accident
LWR	light water reactor
LWRS	Light Water Reactor Sustainability
M&S	modeling and simulation
MAMBA	MPO advanced model for boron analysis
M-CFD	multiphase computational fluid dynamics
MIT	Massachusetts Institute of Technology
MNM	Models and Numerical Methods
MOC	method of characteristics
MPACT	Michigan parallel characteristics transport code
MPO	Materials Performance and Optimization

NCSU	North Carolina State University
NEAMS	Nuclear Energy Advanced Modeling and Simulation
NE-KAMS	Nuclear Energy – Knowledge base for Advanced Modeling and Simulation
NPP	nuclear power plant
NRC	Nuclear Regulatory Commission
NRR	NRC Office of Nuclear Reactor Regulation
NSSS	nuclear steam supply system
OIG	Office of Inspector General
OLCF	Oak Ridge Leadership Computing Facility
OR	operational reactor
ORNL	Oak Ridge National Laboratory
PCI	pellet-cladding interaction
PCM	percent mille (10-5)
PCMI	pellet-cladding mechanical interaction
PF	1015 floating point operations per second (“petaflop”)
PHI	Physics Integration
PoR	plan of record
PWR	pressurized water reactor
QOI	quantity of interest
R&D	research and development
RD&D	research, development, and deployment
RES	NRC Office of Nuclear Regulatory Research
RIA	reactivity insertion accident
RCP	recirculating coolant pump
RMS	records management system
RPV	reactor pressure vessel
RSICC	Radiation Safety Information Computational Center
RTM	Radiation Transport Methods
S&T	science and technology
SA	sensitivity analysis
SBA	station blackout
S/G	steam generator
SLCS	Standby Liquid Control System
SLT	Senior Leadership Team
SMR	small modular reactor
SNL	Sandia National Laboratories
T/H	thermal-hydraulics
TDO	Technology Deployment and Outreach
TF	1012 floating point operations per second (“teraflop”)
THM	Thermal Hydraulics Methods
TLT	Technical Leadership Team
TVA	Tennessee Valley Authority
TWIGL	A computer code for solving neutron diffusion equations
UQ	uncertainty quantification
UM	University of Michigan
V&V	verification and validation
VERA	Virtual Environment for Reactor Applications
VMA	Validation and Modeling Applications
VOCC	Virtual Office, Community, and Computing
VPSC	Viscoplastic Self-Consistent model
VR	virtual reactor
VRI	Virtual Reactor Integration Focus Area
VUQ	Validation and Uncertainty Quantification
VVUQ	Verification, Validation and Uncertainty Quantification

WEC Westinghouse Electric Company

1. INTRODUCTION

The purpose of this report is to describe a series of benchmark calculations performed using the method of characteristics radiation transport code MPACT to verify its radial transport and axial buckling calculation capabilities. The benchmarks are based on a series of Babcock & Wilcox critical assembly configurations as documented in Refs. 1 (which describes what is commonly known as the B&W-1484 benchmark experiment) and 2 (which is commonly referred to as the B&W-1810 benchmark experiment).

The B&W-1484 experiment consists of 21 critical configurations (traditionally identified as I – XXI but identified herein as 4:1 – 4:21) that simulated a variety of close-packed light water reactor (LWR) fuel storage configurations. Criticality measurements were performed and a series of Monte Carlo criticality calculations were also performed at the time to create an analytical basis for comparison with the experimental data. Core 4:1 is a reference "core" containing 438 fuel rods arranged in a roughly cylindrical configuration. All of the remaining cores consist of nine 14 × 14 fuel pin assemblies grouped into a 3 × 3 array and spaced from 0 to 4 pin pitches apart. The following materials were placed within the spaces separating the arrays:

1. Moderator,
2. Moderator and B_4C-bearing pins,
3. Moderator and stainless steel sheets, and
4. Moderator and borated aluminum sheets.

From this set of experiments, Cores 4:1 – 4:3 are the most appropriate to examine MPACT's capabilities with and will be focused upon. The other cases represent configurations that are not appropriate to assess a core simulator with but rather are appropriate for assessing spent fuel pool calculation tools and will not be discussed in depth. However, because many of the input parameters are common between the various cores, where there is the opportunity to inspect and document common parameters, it will be done and those inputs will be made available to future analysts.

Later, the B&W-1810 experiment consisted of 23 critical core configurations (identified herein as 8:1 – 8:23). These experiments were performed to assess the effect of gadolinium (Gd_2O_3) absorbers used to permit higher than then-traditional assembly burnups and was designed to also be usable as a future benchmark.

As noted previously, some of the critical configurations are more relevant than others to the verification of MPACT. Therefore, only a subset of the available 44 core configurations will be examined in-depth. These cores are: 4:1 – 4:3, and 8:1 – 8:10 and 8:12 – 8:17. Due to the similarity of the cases, when the opportunity exists to document relevant details related to other cases, those details will be included herein.

2. METHODOLOGY

All calculations herein are performed with the Michigan PArallel Characteristics-based Transport (MPACT) code. MPACT is a deterministic radiation transport code designed to perform high-fidelity light-water reactor (LWR) analyses using whole-core, pin-resolved, calculations. To permit the use of general and precise geometry, MPACT uses the method of characteristics (MOC), which sweeps rays through the entire geometry on a 2D plane with a fine inter-ray spacing to accumulate and attenuate the neutron flux according to the material properties for the sub region being swept through. MPACT then has a variety of methods to couple the 2D planes together to perform fully-3D calculations. In addition, MPACT uses course-mesh finite difference (CMFD) as an acceleration mechanism. However, because the calculations herein are concerned with the radial transport and axial buckling functionality in MPACT, its 3D capabilities will not be discussed further. At present, MPACT discretizes energy using multiple discrete energy groups that are defined consistent with the cross-section library being used.

Because MPACT is self-contained and intended for generic LWR analyses, user input burden is minimized. Two methods are available to specify geometry: core geometry and subgeometries or core mesh and submeshes. For the B&W-1484 analysis, direct specification of the geometric mesh and submeshes was selected because the benchmark problem provides specific albeit straightforward geometric parameters. Further, specific and explicit material definitions are available in References 1 and 2. Conversely, the B&W-1810 analysis used MPACT's core geometry and subgeometry specification system.

In addition to MPACT, KENO was used herein to rerun the cases prepared as part of the original benchmarking effort for Cores 4:1 and 4:2. KENO is a 3D generalized geometry Monte Carlo computer code within the SCALE package (Reference 13) primarily used for criticality safety analysis. Originally developed to use multigroup nuclear data, the current version is capable of using continuous energy nuclear data. The original cases were modeled using fully-3D geometry and were re-executed as such. They were also collapsed to infinite 2D models to provide a direct comparison with unbuckled MPACT executions. A summary of this analysis is shown in Appendix A.

3. B&W-1484 MODELS

3.1 Geometry

Table 1 lists the key parameters for the B&W-1484 benchmark problem cores considered herein.

Table 1. Summary of Key Model Parameters for B&W-1484 Benchmark

#	Core(s)	Description	Value	Ref.
1	4:All	Core Tank Radius	152.4 / 2 = 76.2 cm	1, Section 3.1; Calculated
2	4:All	Core Tank Wall Thickness	1.27 cm	1, Section 3.1
3	4:All	Core Tank Wall Material	6061-T6 Al	1, Section 3.1 & Assumed
4	4:All	Fuel Pellet OR	1.030 / 2 = 0.515 cm	1, Table 1; Calculated
5	4:All	Fuel Enrichment	2.46 w/o	1, Section 3.2
6	4:All	Clad IR	1.206 / 2 -0.081 = 0.522 cm	1, Table 1; Calculated
7	4:All	Clad OR	1.206 / 2 = 0.603 cm	1, Table 1; Calculated
8	4:All	Clad Material	6061-T6 Al	1, Table 1
9	4:All	Rod & Lattice Pitch	0.644 × 2.54 = 1.636 cm	1, Section 8; Calculated
10	4:4-4:8	B_4C Tube OR	1.113 / 2 = 0.557 cm	1, Section 3.3; Calculated
11	4:4-4:8	B_4C Tube IR	1.113 / 2 – 0.089 = 0.468 cm	1, Section 3.3; Calculated
12	4:4-4:8	B_4C Tube Material	6061-T6 Al	1, Section 3.3 & Assumed
13	4:4-4:8	B_4C Compaction	0.879 ± 0.001 gm/cm	1, Section 3.3
14	4:4-4:8	B_4C Density	0.879 / (3.14 × 0.468^2) = 1.278 gm/cm^3	1, Section 3.3; Calculated
15	4:10-4:19	Threaded Al Rod OR	0.500 × 2.54 / 2 = 0.635 cm	1, Section 3.4; Calculated
16	4:10-4:19	Threaded Al Rod Material	6061-T6 Al	1, Section 3.4 & Assumed
17	4:11 & 4:12	SS Isolation Sheet Thickness	0.462 ± 0.008 cm	1, Section 3.5
18	4:11 & 4:12	SS Isolation Sheet Material	Stainless Steel 304	1, Section 3.5
19	4:13-4:21	Al Isolation Sheet Thickness	0.645 ± 0.005 cm	1, Section 3.6
20	4:13-4:21	Al Isolation Sheet Material	Borated (0.10-1.25%, 1.62%) 6061-T6 Al	1, Section 3.6

Note that the isolation sheets used in Cases 4:11–4:21 are assumed to have no gaps when fit together based on the egg-crate form factor described in Reference 1, Section 3.5. The unit cell geometries are shown in Figures 1, 2, and 3. For the benchmark problems for each case, the unit cell geometries are arranged on a regular Cartesian grid with a square pitch of 1.636 cm. In this way, each of the components (including the isolation sheets) can be fit together appropriately by assuming that each component is centered in its given cell (a reasonable assumption).

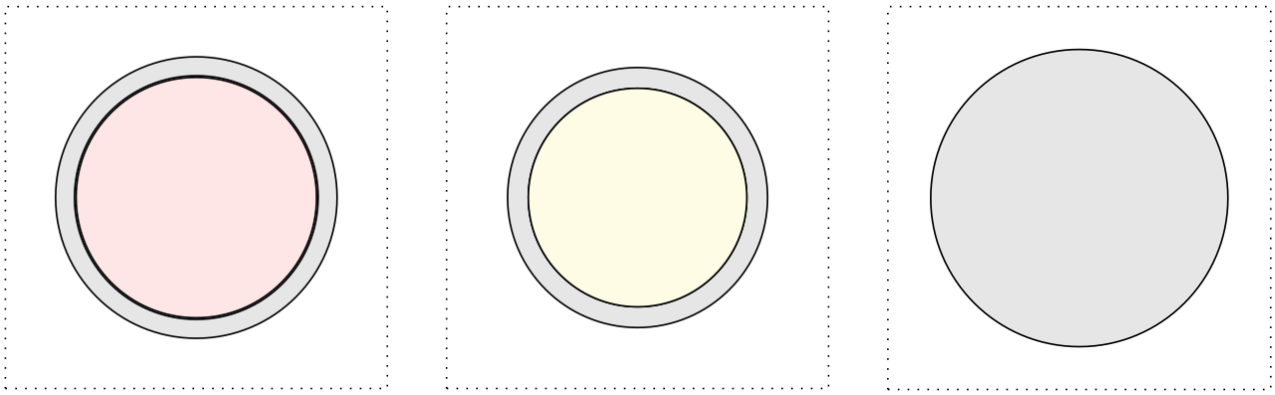

(a) Fuel Pin (b) B_4C Pin (c) Threaded Aluminum Rod

Figure 1: B&W-1484 Benchmark Unit Pin Cell Types

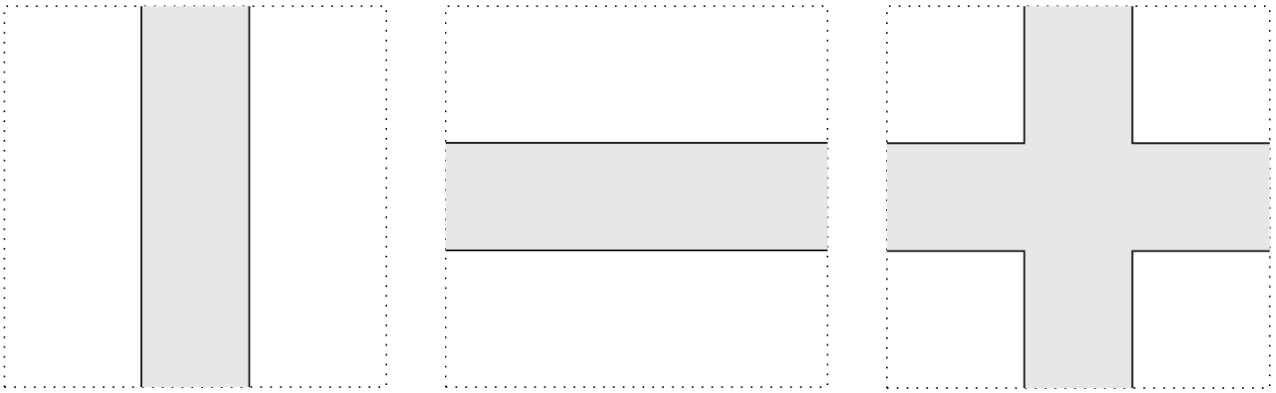

(a) Vertical Sheet (b) Horizontal Sheet (c) Cruciform Sheet

Figure 2: B&W-1484 Benchmark Stainless Steel Isolation Sheet Unit Cell Types

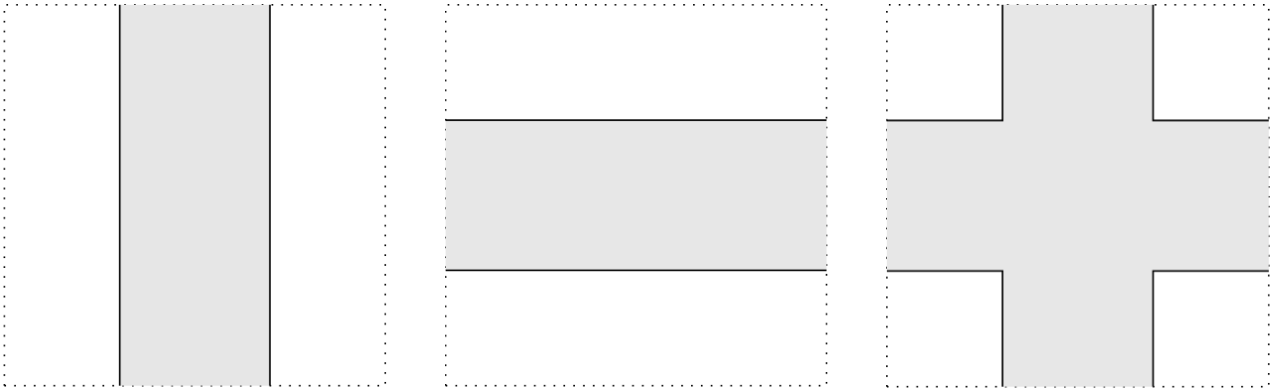

(a) Vertical Sheet (b) Horizontal Sheet (c) Cruciform Sheet

Figure 3: B&W-1484 Benchmark Borated Aluminum Isolation Sheet Unit Cell Types

Also, one should recognize that the gap between the fuel pellet and clad is small to the point where resolving it in the model runs the risk of inadequate ray intersections for even relatively fine ray separation (e.g., 0.05 cm).

Because we know that the radius of the core tank is 76.2 cm, we know that the maximum amount of pin pitches along the diagonal is

$$76.2\text{ cm} = \sqrt{(n \times 1.636\text{ cm})^2 + (n \times 1.636\text{ cm})^2} \Longrightarrow n \approx 32$$

and along the cardinal axes

$$n = \frac{76.2\text{ cm}}{1.636\text{ cm}} \approx 46.$$

With these values in mind, we can size our 2D model to include as much of the moderator as possible without needing to represent the cylindrical moderator tank (which would need to be approximated on the overall Cartesian mesh). When the cases are executed, the flux distribution will be assessed to ensure that the model size is appropriate to account for any boundary effects.

The material distribution plan views of Cores 4:1, 4:2 and 4:3 are shown in Figures 4, 5, and 6, respectively. In these figures, the fuel is red, the cladding is green, and the moderator as blue. Taking advantage of geometric symmetry, Core 4:1 is a half-core reflective model whereas Cores 4:2 and 4:3 are quarter-core reflective models. Note that Core 4:1 is not able to be made quarter-core reflective due to an asymmetry of the outer-most row of pins on the north/south flats.

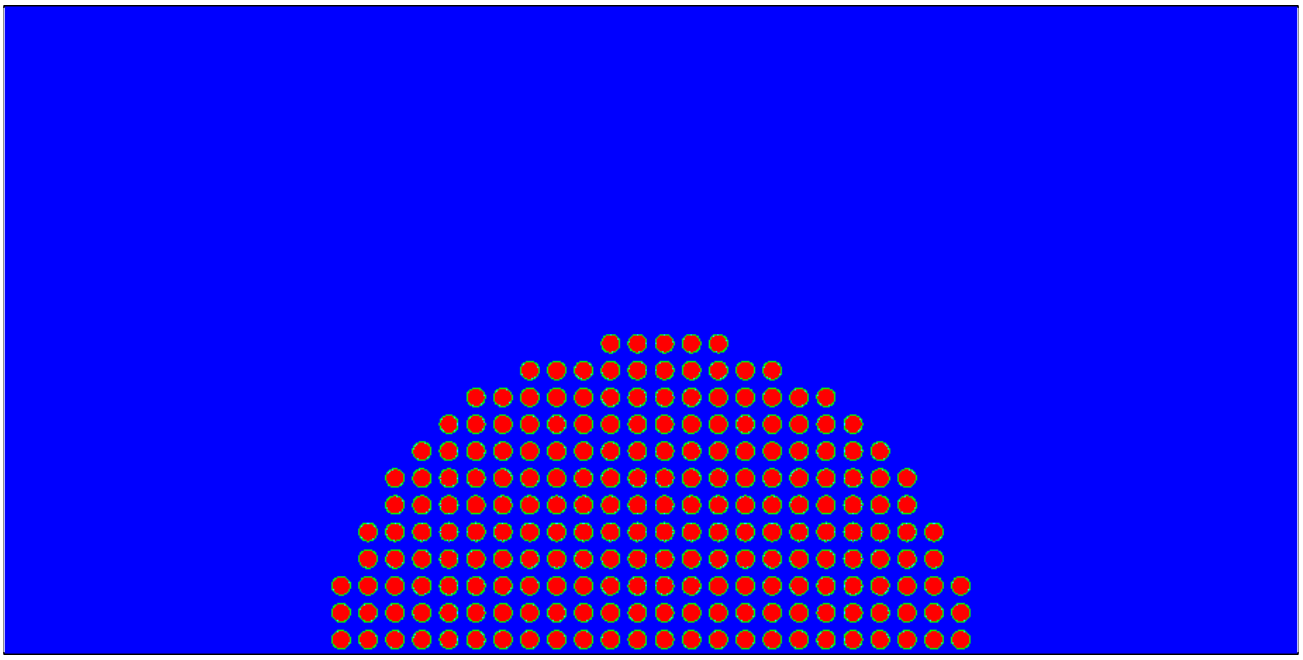

Figure 4: B&W-1484 Core 4:1

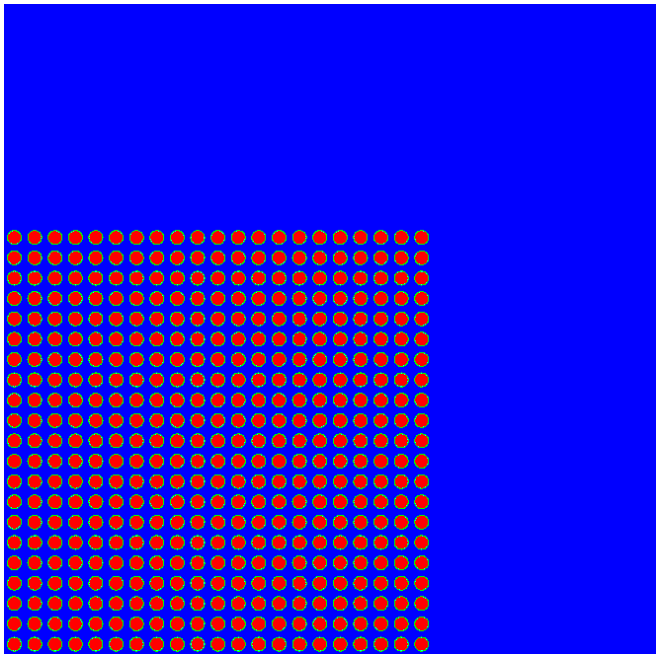

Figure 4: B&W-1484 Core 4:2

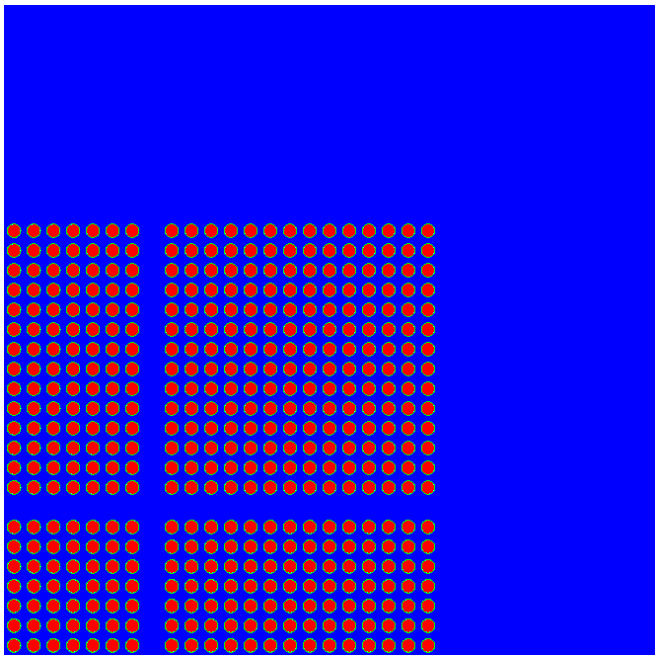

Figure 4: B&W-1484 Core 4:3

3.2 Materials

The cases documented herein primarily use a 47-group library being developed within CASL that is appropriate for reactor physics calculations (mpact47g_70s_v4.0_11032014.fmt). For the P1-outscatter transport correction, the library mpact47g_e70r0_Pn.xsl is used instead.

Using these libraries, there are a variety of materials needed for the different cases of this benchmark. These materials are given in Table 10 of Reference 1. Despite the fact that no single case requires all of the materials, all materials are included in each input file to allow future analysts (and this analyst) to easily compare input decks using the *nix `diff` command.

From the values specified in Table 10 of Reference 1, some adjustments were necessary based on the nuclides available in the nuclear data libraries used for this analysis. These adjustments were:

- For aluminum type 6061, no natural copper nuclear data are available so the number density given for copper (1.02328e-4 a/b-cm) was split according to the natural abundances of Cu-63 and Cu-65 (69.15% and 30.85%, respectively, from Reference 3). The resulting number densities for Cu-63 and Cu-65 are 7.07598e-5 and 3.15682e-5 a/b-cm, respectively.
- For the moderator based on borated water (143 ppm) at 24.5 °C, the water constituent components need to be multiplied by 0.997947 giving
  - 6.66683e-2 (0.997947) = 6.65314e-2 a/b-cm Hydrogen,
  - 3.33342e-2 (0.997947) = 3.32658e-2 a/b-cm Oxygen, and
  - 7.96720e-6 (0.997947) = 7.95084e-6 a/b-cm Boron.
- For the moderator based on borated water (514 ppm) at 26 °C, the water constituent components need to be multiplied by 0.997947 giving
  - 6.66424e-2 (0.997947) = 6.65056e-2 a/b-cm Hydrogen,
  - 3.33212e-2 (0.997947) = 3.32528e-2 a/b-cm Oxygen, and
  - 2.86260e-5 (0.997947) = 2.85672e-5 a/b-cm Boron.
- For the moderator based on borated water (217 ppm) at 26 °C, the water constituent components need to be multiplied by 0.997947 giving

  - 6.66424e-2 (0.997947) = 6.65056e-2 a/b-cm Hydrogen,
  - 3.33212e-2 (0.997947) = 3.32528e-2 a/b-cm Oxygen, and
  - 1.20820e-5 (0.997947) = 1.20572e-5 a/b-cm Boron.
- For stainless steel 304, no natural copper nuclear data are available so the number density given for copper (5.3252e-5 a/b-cm) was split according to the natural abundances of Cu-63 and Cu-65 (69.15% and 30.85%, respectively, from Reference 3). The resulting number densities for Cu-63 and Cu-65 are 3.68238e-5 and 1.64282e-5 a/b-cm, respectively.
- For the moderator based on borated water (15 ppm) at 20 °C, the water constituent components need to be multiplied by 0.997947 giving
  - 6.67373e-2 (0.997947) = 6.66003e-2 a/b-cm Hydrogen,
  - 3.33687e-2 (0.997947) = 3.33002e-2 a/b-cm Oxygen, and
  - 8.36585e-7 (0.997947) = 8.34867e-7 a/b-cm Boron.
- For the moderator based on borated water (92 ppm) at 18 °C, the water constituent components need to be multiplied by 0.997947 giving
  - 6.67635e-2 (0.997947) = 6.66264e-2 a/b-cm Hydrogen,
  - 3.33818e-2 (0.997947) = 3.33133e-2 a/b-cm Oxygen, and
  - 5.13310e-6 (0.997947) = 5.12256e-6 a/b-cm Boron.
- For the moderator based on borated water (395 ppm) at 18 °C, the water constituent components need to be multiplied by 0.997947 giving
  - 6.67635e-2 (0.997947) = 6.66264e-2 a/b-cm Hydrogen,
  - 3.33818e-2 (0.997947) = 3.33133e-2 a/b-cm Oxygen, and
  - 2.20390e-5 (0.997947) = 2.19938e-5 a/b-cm Boron.
- For the moderator based on borated water (121 ppm) at 17.5 °C, the water constituent components need to be multiplied by 0.997947 giving
  - 6.67695e-2 (0.997947) = 6.66324e-2 a/b-cm Hydrogen,
  - 3.33848e-2 (0.997947) = 3.33163e-2 a/b-cm Oxygen, and
  - 6.75170e-6 (0.997947) = 6.73784e-6 a/b-cm Boron.
- For the moderator based on borated water (487 ppm) at 17.5 °C, the water constituent components need to be multiplied by 0.997947 giving
  - 6.67695e-2 (0.997947) = 6.66324e-2 a/b-cm Hydrogen,
  - 3.33848e-2 (0.997947) = 3.33163e-2 a/b-cm Oxygen, and
  - 2.71740e-6 (0.997947) = 2.71182e-6 a/b-cm Boron.
- For the moderator based on borated water (197 ppm) at 18 °C, the water constituent components need to be multiplied by 0.997947 giving
  - 6.67635e-2 (0.997947) = 6.66264e-2 a/b-cm Hydrogen,
  - 3.33818e-2 (0.997947) = 3.33133e-2 a/b-cm Oxygen, and
  - 1.09910e-5 (0.997947) = 1.09684e-5 a/b-cm Boron.
- For the moderator based on borated water (634 ppm) at 17.5 °C, the water constituent components need to be multiplied by 0.997947 giving
  - 6.67695e-2 (0.997947) = 6.66324e-2 a/b-cm Hydrogen,
  - 3.33848e-2 (0.997947) = 3.33163e-2 a/b-cm Oxygen, and
  - 3.53770e-5 (0.997947) = 3.53044e-5 a/b-cm Boron.
- For the moderator based on borated water (320 ppm) at 17.5 °C, the water constituent components need to be multiplied by 0.997947 giving
  - 6.67695e-2 (0.997947) = 6.66324e-2 a/b-cm Hydrogen,
  - 3.33848e-2 (0.997947) = 3.33163e-2 a/b-cm Oxygen, and
  - 1.78560e-5 (0.997947) = 1.78193e-5 a/b-cm Boron.

- For the moderator based on borated water (72 ppm) at 16.5 °C, the water constituent components need to be multiplied by 0.997947 giving
  - 6.67812e-2 (0.997947) = 6.66441e-2 a/b-cm Hydrogen,
  - 3.33906e-2 (0.997947) = 3.33220e-2 a/b-cm Oxygen, and
  - 4.01830e-6 (0.997947) = 4.01005e-6 a/b-cm Boron.

Note that there is a typo on Page 8-11 of Reference 1 where the number density for oxygen for borated water (92 ppm) at 18 °C is given as 3.33813e-2 a/b-cm when it should instead be 3.33818e-2 a/b-cm.

An additional material was created that was not specified in Reference 1 to act as the backfill gas in the fuel rods. This material was chosen to be dry air near sea level at atmospheric pressure (0.00121 gm/cm^3) as specified in Reference 4 with carbon and argon removed because of their low abundance (and because of argon's poor availability in typical reactor physics cross section libraries). If this region was instead backfilled with helium gas (modern common practice), the difference is not expected to be significant.

For 3D models, the material below the fuel has historically been modeled as a smear of 82.44% aluminum and 17.56% (borated) water (Reference 1, Section 7.3); however, because the MPACT models considered herein are 2D, this detail is provided for reference and not for use in any manner.

3.2.1 Core 3 Subcases

Rather than calculating them explicitly, for convenience the known boron number densities and concentrations for 17.5 °C and 18 °C were plotted and a least-squares fit was used to derive a fitting equation. For 17.5 °C, that equation is

$$f(x) = 5.57954 \times 10^{-8}x - 3.24568 \times 10^{-10}$$

with a linear regression value of 1.00000 whereas for 18 °C, that equation is

$$f(x) = 5.57954 \times 10^{-8}x - 1.22622 \times 10^{-11}$$

again with a linear regression value of 1.00000. As such, the number density values for the various concentrations of boron at 18.5 °C are calculated (extrapolated) from

$$f(x) = 5.57954 \times 10^{-8}x - \frac{3.24568 \times 10^{-10} + 1.22622 \times 10^{-11}}{2}$$

which is deemed accurate enough for the purposes herein. The resulting values are shown in Table 2.

Table 2. Core 3 Subcase Boron Number Densities

Subcase	Moderator Temperature (°C)	Natural Boron Concentration (ppm)	Moderator Height (cm)	Natural Boron Number Density (a/bn-cm)
3a	18.0	769	148.63	4.29065e-5
3b	18.0	764	144.88	4.26275e-5
3c	18.0	762	140.38	4.25159e-5
3d	18.5	753	131.32	4.20138e-5
3e	18.0	739	120.64	4.12327e-5
3f	18.0	721	110.04	4.02283e-5
3g	18.5	702	100.32	3.91682e-5

3.2.2 Material Temperature & Density Calculations

Each case is assumed to have all materials at thermal equilibrium. That is, all material temperatures are set equal to the moderator temperature specified in Table 10 of Reference 1. Moderator densities, while not varying much, were set accordingly assuming atmospheric pressure as retrieved from `http://www.wolframalpha.com/` with a query in the form `density of water at atmospheric pressure 21 C`. The summary of system temperatures and moderator densities are summarized in Table 3.

Table 3. Summary of System Temperature and Moderator Mass Density Values

Core	System Temperature (°C)	Moderator Mass Density (gm/cm^3)
4:1	21.00	0.9980
4:2	18.50	0.9985
4:3	18.00	0.9986
4:4	17.00	0.9988
4:5	17.50	0.9987
4:6	17.50	0.9987
4:7	17.50	0.9987
4:8	17.50	0.9987
4:9	17.50	0.9987
4:10	24.50	0.9972
4:11	26.00	0.9968
4:12	26.00	0.9968
4:13	20.00	0.9982
4:14	18.00	0.9986
4:15	18.00	0.9986
4:16	17.50	0.9987
4:17	17.50	0.9987
4:18	18.00	0.9986
4:19	17.50	0.9987
4:20	17.50	0.9987
4:21	16.50	0.9989

The fuel pellet density is taken to be the density given in Table 1 of Reference 1: 10.22 g/cm^3. The density for all aluminum components is taken to be the density given for the sheets on Page 8-3 of Reference 1: 2.70 g/cm^3. The density of stainless steel 304 is taken to be 8.00 g/cm^3 from Reference 4. For those regions that are smeared with moderator and aluminum, the density was kept consistent with the moderator because it occupies the overwhelming fraction (~99.8%) of the material.

3.3 Geometric Buckling

All cases run with MPACT are 2D in nature in order to strictly assess MPACT's radial transport capabilities. Correspondingly, axial buckling must be used to represent the axial leakage effect that would have existed in the physical system and the 3D KENO computational models and so MPACT's axial buckling capabilities are also being exercised. Buckling values applied historically for Cores 4:1 and 4:3 are available in Reference 5 and were reused herein without modification. The buckling value for Core 4:2 was assumed to be the same as Core 4:1 because of the similar moderator height. All buckling values used are summarized in Table 4. The buckled heights, H_B, corresponding to the buckling values assuming slab geometry are calculated as

$$H_B = \pi / \sqrt{B^2}$$

which gives extrapolation lengths, ℓ, calculated as

$$\ell = H_B - H$$

relative to the critical heights where both values are also given in Table 4.

Table 4. Summary of Geometric Buckling & Critical Height Values

Core	Geometric Buckling (cm^{-2})	Critical Height (cm)	Buckled Height (cm)	Extrapolation (cm)
4:1	4.10e-4	143.88	147.93	11.27
4:2	4.10e-4	144.29	147.93	10.86
4:3a	3.87e-4	148.63	159.70	11.07
4:3b	4.06e-4	144.88	155.92	11.04
4:3c	4.31e-4	140.38	151.33	10.95
4:3d	4.87e-4	131.32	142.36	11.04
4:3e	5.69e-4	120.64	131.70	11.06
4:3f	6.73e-4	110.04	121.10	11.06
4:3g	7.96e-4	100.32	111.35	11.03

We note that the extrapolation lengths resulting from the various buckling values for Cores 4:1, 4:2, and 4:3 are self-consistent (~11 cm). However, Core 4:2 has a somewhat lower extrapolated length than Core 4:1. Because it is an assumed buckling value, it is not changed but this difference should be recognized when assessing any discrepancies. Additional work to rigorously develop a method to (re-)compute the buckling for the various cores is recommended.

Note that in Core 4:3b, a buckling value of 4.05e-4 cm^{-2} was used in the executions, rather than the historic value of 4.06e-4 cm^{-2} because of instabilities witnessed within MPACT. The effect of this difference is negligible and the instabilities are currently being investigated.

3.4 Results

The B&W-1484 benchmark summary report (Reference 1) only provides system eigenvalues for comparison (corresponding to critical, for all cores) so there is a dearth of information with which to compare. Regardless, the eigenvalues for Cores 4:1 and 4:2 are shown in Table 5 and the eigenvalues for the various Core 4:3 configurations are shown in Table 6. Within these tables, the effect of different scattering methods is apparent. The scattering methods used include:

1. P_0 & P_2, which are standard scattering expansions for neutron transport calculations,
2. TCP_0 (NLC), which calculates a diffusion coefficient based on a total neutron leakage conservation through a uniform slab of hydrogen (discussed in more detail in Reference 15),
3. Limited TCP_0 (NLC), which is identical to TCP_0 (NLC) but truncates any negative cross sections with a group upper-bound energy over 1 MeV, and
4. TCP_0 (Out-scatter), which performs a traditional out-scatter correction whereby the transport-corrected cross section is the total cross section for a given group with all first-moment scattering to other groups subtracted out.

With these different scattering methods, we can observe from the Core 4:1 and 4:2 cases that the TCP_0 (Out-scatter) gives the least desirable results (excluding P_0). For P_2, we see comparable levels of agreement for Core 4:1 (~130 pcm) and Core 4:2 (~90 pcm) but with Core 4:1 overreactive and Core 4:2 underreactive. Furthermore, for P_2 and the NLC-based transport-corrected scattering methods, we observe a relatively consistent ~270 pcm negative bias in Core 4:2 relative to Core 4:1. Other than core geometry (in 2D), the only way in which these cases different is that Core 4:1 has

unborated moderator whereas Core 4:2 has 1037 ppm of dissolved boron. In prior analyses, discrepancies have been observed based on the use of a historic B-10:B-11 ratio versus a modern one (i.e., 19.9:80.1, respectively). However, it was confirmed that this was not the case herein. Furthermore, the MPACT calculation uses the same abundances as the historic KENO executions.

The radial and azimuthal mesh definitions for Cores 4:1 and 4:2 are consistent and a sensitivity study was performed wherein no significant changes (i.e., improvements) were observed when varying the mesh spacing. A similar sensitivity study was performed in the ray spacing without significant improvement in the calculated effective eigenvalues.

As noted previously, the buckling value for Core 4:1 was reused directly from Reference 5 and Core 4:2 is assumed to be the same because no historic value is available for comparison. Because the buckling, and thus leakage, will directly influence the eigenvalue, it is recommended that additional work be performed to develop a rigorous method to (re-)compute the buckling values on a core-wise basis for this benchmark problem. Additional discussion on the impact of buckling is given in Appendix B.

For the various Core 4:3 configurations, the agreement between the calculated and measured eigenvalues for the TCP_0 (NLC) was generally within 100 pcm. The Limited TCP_0 cases were generally within 50 pcm; however, this method uses an *ad hoc* truncation to control cross section negativity and so the results might be believed to be more physically appropriate but less rigorously developed. Furthermore, these cases demonstrate a behavior expected, those cases executed with TCP_0 (NLC) exhibit lower eigenvalues (~210 pcm) than Limited TCP_0 cases because of the negative cross section truncation. Both of these cases are lower than the P_2-calculated cases (again with Limited TCP_0 ~100 pcm lower than P_2), which are known to have strictly non-negative cross sections. Regardless, the Core 4:3 configurations along with Cores 4:1 and 4:2 demonstrate the effect of negativity in the cross sections, leading to negativity in the flux solution, that ultimately influences the calculated system eigenvalue. In these NLC-based transport-corrected solutions, no negative fluxes were observed in the final converged solution; however, the effect of negativity enroute to the solution is apparent.

In summary, the benchmark models for Cores 4:1 and 4:3 produce effective eigenvalues within 200 pcm of measured values for P_2 and NLC-based transport-corrected scattering treatments are used. Core 4:2 results also fall within 200 pcm for P_2 and truncated NLC-based transport-corrected scattering and nearly so (254 pcm) with standard NLC-based transport-correction. The major unknown is the applied buckling value which has a direct impact on the effective eigenvalue, the only value available for comparison with the original benchmark cases (where no buckling was applied). As such, additional effort to rigorously calculate this buckling value is suggested on a case-by-case basis using a more physically-appropriate method than a slab approximation. In addition, an improved transport-correction method that can eliminate non-physical negative cross sections (and thus non-physical negative fluxes) should be pursued.

Table 5. B&W-1484 Core 4:1 and 4:2 MPACT-Calculated Eigenvalues

Calculated Effective Eigenvalue		
Scattering Method	**Core 4:1**	**Core 4:2**
P_0	1.10110	1.03842
P_2	1.00132	0.99910
TCP_0 (NLC)	0.99977	0.99746
Limited TCP_0 (NLC)	1.00192	0.99844
TCP_0 (Out-scatter)	0.99292	0.99497
Distance from Critical (pcm)		
Scattering Method	**Core 4:1**	**Core 4:2**
P_0	10110	3842
P_2	132	-90
TCP_0 (NLC)	-23	-254
Limited TCP_0 (NLC)	192	-156
TCP_0 (Out-scatter)	-708	-503

Table 6. B&W-1484 Core 4:3 Subcase MPACT-Calculated Eigenvalues

Calculated Effective Eigenvalue			
Core	**P_2**	**TCP_0 (NLC)**	**Limited TCP_0 (NLC)**
4:3a	1.00155	0.99960	1.00054
4:3b	1.00191	0.99997	1.00090
4:3c	1.00139	0.99944	1.00039
4:3d	1.00121	0.99926	1.00023
4:3e	1.00112	0.99918	1.00017
4:3f	1.00108	0.99915	1.00016
4:3g	1.00060	0.99867	0.99971
Distance from Critical (pcm)			
Core	**P_2**	**TCP_0 (NLC)**	**Limited TCP_0 (NLC)**
4:3a	155	-40	54
4:3b	191	-3	90
4:3c	139	-56	39
4:3d	121	-74	23
4:3e	112	-82	17
4:3f	108	-85	16
4:3g	60	-133	-29

4. B&W-1810 MODELS

4.1 Geometry

Table 7 lists the key parameters for the B&W-1810 benchmark problem cores considered herein. The various pin type locations can be found in Pages 4–46 to 4–68 of Reference 2.

Table 7. Summary of Key Model Parameters for B&W-1810 Benchmark

#	Description	Value	Ref.
1	Core Tank Radius	152.4 / 2 = 76.2 cm	2, Section 3.2; Calculated
2	Core Tank Wall Thickness	0.5 × 2.54 = 1.27 cm	2, Section 3.2; Calculated
3	Core Tank Wall Material	6061-T6 Al	2, Section 3.2
4	UO_2 Fuel Enrichment	2.46 w/o	2, Section 3.3
5	UO_2 Fuel Enrichment	4.02 w/o	2, Section 3.4
6	UO_2-Gd_2O_3 Fuel Enrichment	1.944 w/o (4 w/o Gd, 96 w/o U)	2, Section 3.5
7	Ag-In-Cd Rod Composition	80 w/o Ag, 15 w/o In, 5 w/o Cd	2, Section 3.7
8	Fuel Pellet OR (2.46 w/o)	0.4054 / 2 × 2.54 = 0.515 cm	2, Table 3--1; Calculated
9	Fuel Pellet OR (4.02 w/o)	0.444 / 2 × 2.54 = 0.564 cm	2, Table 3--2; Calculated
10	Solid Fuel Pellet OR (UO_2-Gd_2O_3)	0.4055 / 2 × 2.54 = 0.515 cm	2, Section 3.5; Calculated
11	Annular Fuel Pellet OR (UO_2-Gd_2O_3)	0.4055 / 2 × 2.54 = 0.515 cm	2, Section 3.6; Calculated
12	Annular Fuel Pellet IR (UO_2-Gd_2O_3)	0.130 / 2 × 2.54 = 1.65 cm	2, Section 3.6; Calculated
13	Ag-In-Cd OR	0.400 / 2 × 2.54 = 0.508 cm	2, Section 3.7; Calculated
14	Clad Material (UO_2 2.46 w/o)	6061-T6 Al	2, Section 3.3 & Assumed
15	Clad Material (UO_2 4.02 w/o)	Swaged Stainless Steel 304	2, Section 3.4 & Table 3--2
16	Clad Material (UO_2-Gd_2O_3)	6063 Al Specified, 6061-T6 Al Used	2, Section 3.5 & Assumed
17	Clad IR (2.46 w/o)	0.4748 / 2 × 2.54 – 0.032 × 0.254 = 0.522 cm	2, Table 3--1; Calculated
18	Clad OR (2.46 w/o)	0.4748 / 2 × 2.54 = 0.603 cm	2, Table 3--1; Calculated
19	Clad IR (4.02 w/o)	Fuel Pellet OR (4.02 w/o)	Assumed due to swaging.
20	Clad OR (4.02 w/o)	0.4755 / 2 × 2.54 = 0.604 cm	2, Section 3.4; Calculated
21	Clad IR (UO_2-Gd_2O_3)	0.475 / 2 × 2.54 – 0.032 × 2.54 = 0.522 cm	2, Section 3.5; Calculated
22	Clad OR (UO_2-Gd_2O_3)	0.475 / 2 × 2.54 = 0.603 cm	2, Section 3.5; Calculated
23	Clad Material (Ag--In--Cd)	6063 Al Specified, 6061-T6 Al Used	2, Section 3.7 & Assumed
24	Clad IR (Ag--In--Cd)	0.475 / 2 × 2.54 – 0.032 × 2.54 = 0.522cm	2, Section 3.7; Calculated
25	Clad OR (Ag--In--Cd)	0.475 / 2 × 2.54 = 0.603 cm	2, Section 3.7; Calculated
26	B_4C Tube OR	0.438 / 2 × 2.54 = 0.556 cm	2, Section 3.8; Calculated
27	B_4C Tube IR	0.438 / 2 × 2.54 – 0.035 × 2.54 = 0.467 cm	2, Section 3.8; Calculated
28	B_4C Tube Material	6061-T6 Al	2, Section 3.8 & Assumed
29	B_4C Compaction	2.233 / 2.54 = 0.879 gm/cm	2, Section 3.8; Calculated
30	B_4C Density	0.879 / (3.14 × 0.467^2) = 1.284 gm/cm^3	2, Section 3.8; Calculated
31	Clad Material (Void Tube)	6063 Al Specified, 6061-T6 Al Used	2, Section 3.9 & Assumed
32	Clad IR (Void Tube)	0.475 / 2 × 2.54 – 0.032 × 2.54 = 0.522 cm	2, Section 3.9; Calculated
33	Clad OR (Void Tube)	0.475 / 2 × 2.54 = 0.603 cm	2, Section 3.9; Calculated
34	Rod & Lattice Pitch	0.644 × 2.54 = 1.636 cm	2, Section 4.2; Calculated

The unit cell geometries are shown in Figures 4, 5, and 6. For the benchmark problems for each case, the unit cell geometries are arranged on a regular Cartesian grid with a square pitch of 1.636 cm. In this way, each of the components can be fit together appropriately by assuming that each component is centered in its given cell (a reasonable assumption).

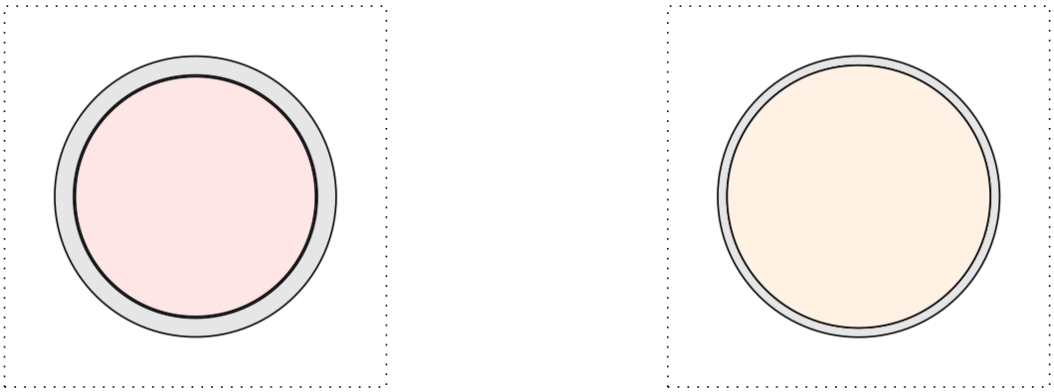

(a) 2.46 w/o Fuel Pin (b) 4.02 w/o Fuel Pin

Figure 4: B&W-1810 Benchmark Unit Pin Cell Types

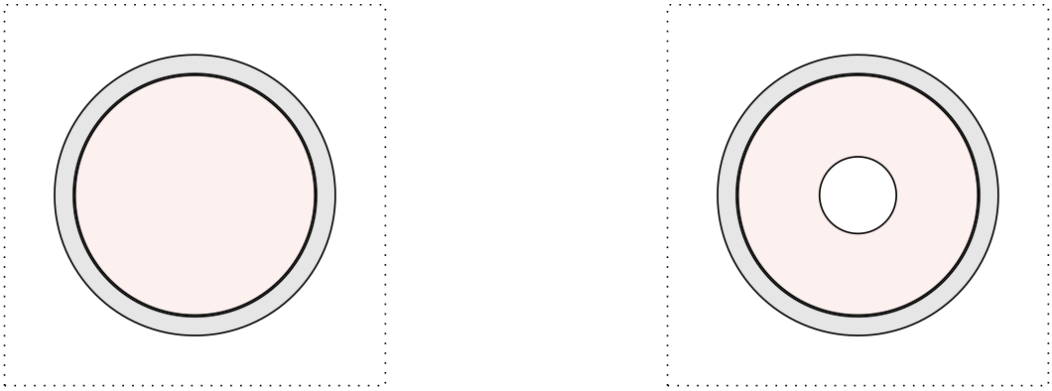

(a) Solid UO_2-Gd_2O_3 Pin (b) Annular UO_2-Gd_2O_3 Pin

Figure 5: B&W-1810 Benchmark Homogenized Absorber & Fuel Unit Cell Types

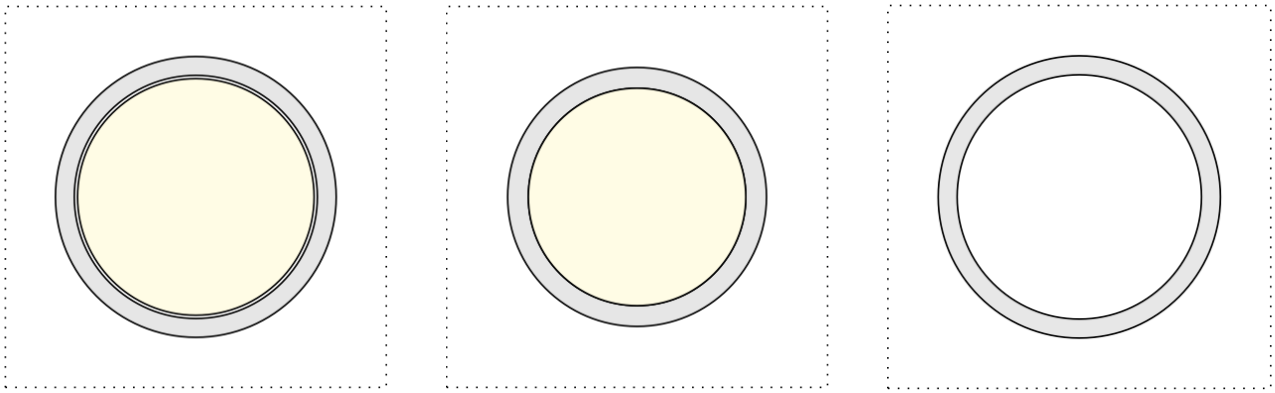

(a) Fuel Pin (b) B_4C Pin (c) Threaded Aluminum Rod

Figure 6: B&W-1810 Benchmark Absorber and Void Unit Cell Types

Also, one should recognize that the gap between the fuel pellet and clad, as appropriate, is small to the point where resolving it in the model runs the risk of inadequate ray intersections for even relatively fine ray separation (e.g., 0.05 cm).

Because we know that the radius of the core tank is 76.2 cm, we know that the maximum amount of pin pitches along the diagonal is

$$76.2\text{ cm} = \sqrt{(n \times 1.636\text{ cm})^2 + (n \times 1.636\text{ cm})^2} \Longrightarrow n \approx 32$$

and along the cardinal axes

$$n = \frac{76.2 \text{ cm}}{1.636 \text{ cm}} \approx 46.$$

Table 8 shows a summary of 19 different core configurations assessed in this work, all of which have varying layouts of fuel and burnable absorber rods. Additionally, select cases also have control rods inserted, of which there are two types (Ag-In-Cd also commonly referred to as AIC and B_4C). Lastly, the boron concentration of the coolant was adjusted in the experiment until a critical configuration was obtained. While it is reasonable to simulate these cases in 3D, it is possible, and even common, to simulate these cases in 2D with a prescribed axial buckling value to account for the 3D effect. All of the B&W-1810 cases used a buckling value of 4.1×10^{-4} cm^2. Lastly, all cases were run using a version of the 47-group library being developed with CASL (mpact47g_70s_v4.0_11032014.fmt).

It should be noted that Core 8:11 did not conform to the same geometric layout as the rest of these cores do, and was set up specifically got resonance integral measurements. This case was not modeled. Additionally, Cores 8:18 – 8:20 have slightly different configurations with 16×16 assemblies and large water holes. These are prime candidates for future evaluation, but have also been omitted.

Table 8. B&W-1810 Benchmark Configuration Summary

Core	Short Description	2.46% Pins	4.02% Pins	Gd Pins	B_4C Pins	AIC Pins	Water Holes	Boron (ppm)
1	0 Gd	4808	0	0	0	0	153	1337.9
2	0 Gd, AIC Rods	4808	0	0	0	16	137	1250.0
3	20 Gd	4788	0	20	0	0	153	1329.3
4	20 Gd, AIC Rods	4788	0	20	0	16	137	1171.7
5	28 Gd	4780	0	28	0	0	153	1208.0
5A	32 Gd	4776	0	28	0	0	153	1191.3
5B	28 Gd	4780	0	32	0	0	153	1207.1
6	28 Gd, AIC Rods	4780	0	28	0	16	137	1155.8
6A	32 Gd, AIC Rods	4776	0	32	0	16	137	1135.6
7	28 Gd (annular)	4780	0	28 (ann.)	0	0	153	1208.8
8	36 Gd	4772	0	36	0	0	153	1170.7
9	36 Gd, AIC Rods	4772	0	36	0	16	137	1130.5
10	36 Gd, Void Rods	4772	0	36	0	0	137	1177.1
12	0 Gd	3920	0	0	0	0	153	1899.3
13	0 Gd, B4C Rods	3920	888	0	16	0	137	1635.4
14	28 Gd	3920	888	28	0	0	153	1653.8
15	28 Gd, B4C Rods	3920	860	28	16	0	137	1479.7
16	36 Gd	3920	852	36	0	0	153	1579.4
17	36 Gd, B4C Rods	3920	852	36	16	0	137	1432.1

Figures 7-10 show the layout of Cores 8:1, 8:5, 8:12, and 8:14 (Reference 2). These cores have been selected for illustration since all of the midplane fission rate comparison data are only available for these four cores. However, detailed layouts of all cores can be found in the benchmark specification.

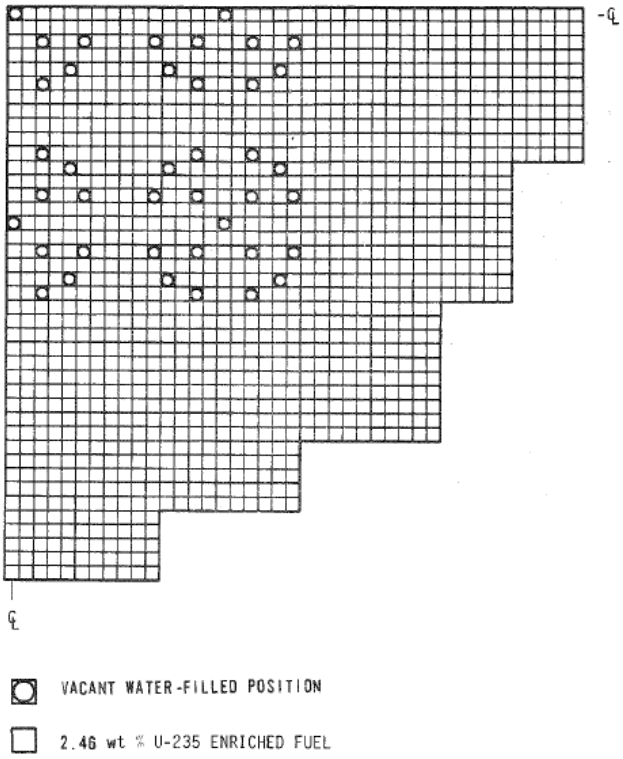

Figure 7: B&W-1810 Core 8:1 Layout

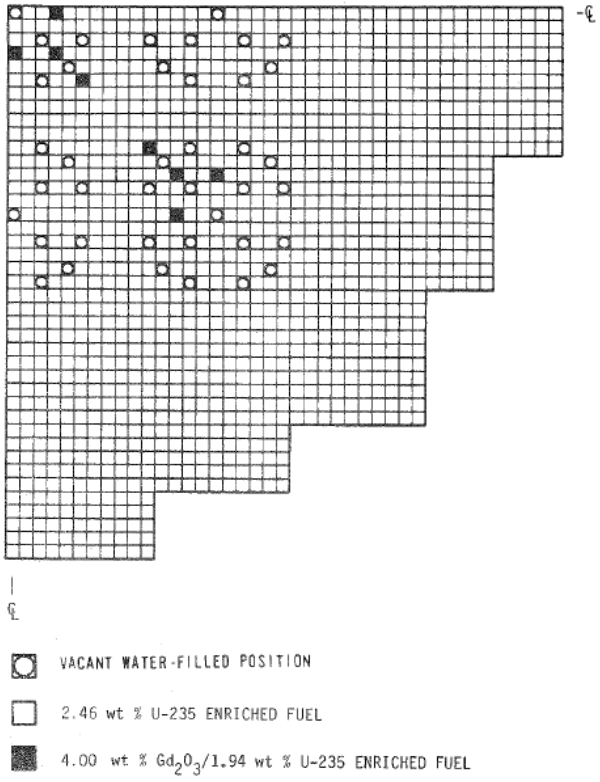

Figure 8: B&W-1810 Core 8:5 Layout

Whereas Cores 8:1 – 8:10 have a uniform 2.46% enrichment, Cores 8:12 – 8:17 have an inner zone with 4.02% enriched fuel and 2.46% in the outer zone.

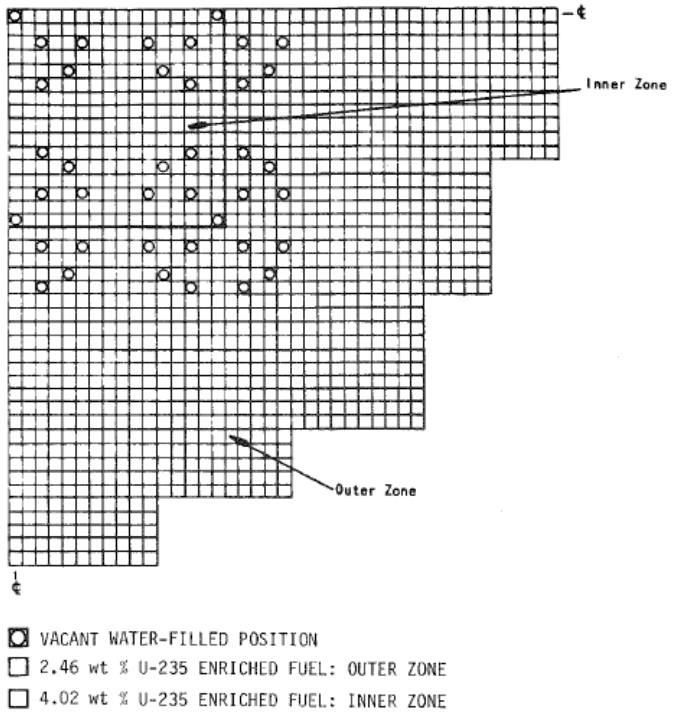

Figure 9: B&W-1810 Core 8:12 Layout

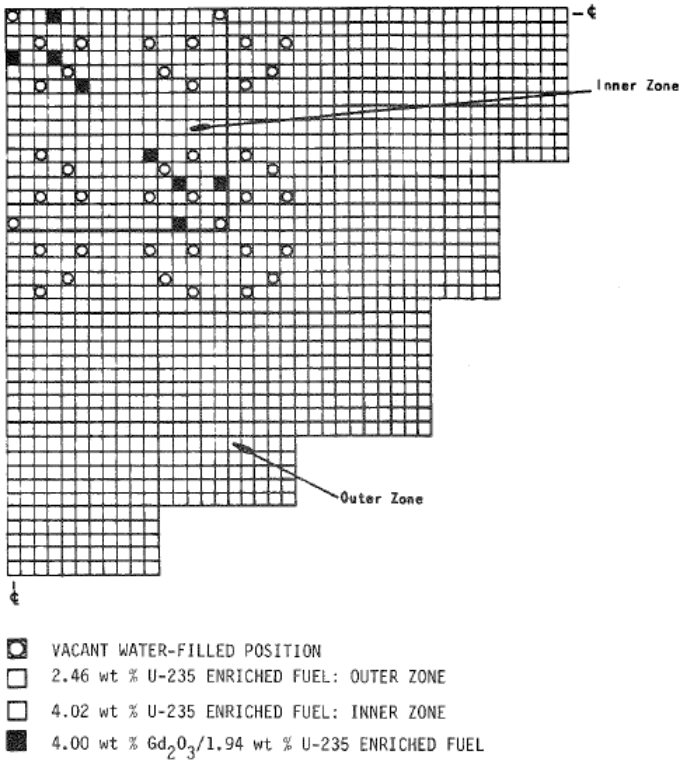

Figure 10: B&W-1810 Core 8:14 Layout

4.2 Materials

As noted in the previous section, there are a variety of materials used in these cases, including three different fuel compositions, two burnable absorber materials, and a handful of different metals for fuel rod cladding and detector modeling. For clarity, both the VERA input card used to describe the material and the output from MPACT (which echoes the material in terms of atomic number density) are included.

4.2.1 2.46% Enriched UO_2

The 2.46% enriched UO_2 fuel has a density of 10.24 g/cc. While the benchmark typically refers to this as 2.46% enriched, it also specifies that is actually slightly less at 2.459% enriched. Fuel rods with this fuel have 6061 aluminum cladding, which is included below.

VERA Input:

```
fuel U246  10.24 99.2 / 2.459
```

MPACT Echo:

```
+-----------------------------------------+
| XS Record Name | Number Density (#/b-cm) |
+-----------------------------------------+
            92234     4.761010513911410E-06
            92235     5.687201837436397E-04
            92236     2.605010930943693E-06
            92238     2.226716926770611E-02
             8001     4.568633092792913E-02
```

4.2.2 4.02% Enriched UO_2

The 4.02% enriched fuel has a density of 9.46 g/cc and these pins are surrounded by 304 stainless steel.

VERA Input:

```
fuel U402  9.46  99.2 / 4.02
```

MPACT Echo:

```
+-----------------------------------------+
| XS Record Name | Number Density (#/b-cm) |
+-----------------------------------------+
            92234     7.492293304533844E-06
            92235     8.589087751332577E-04
            92236     3.934213716800616E-06
            92238     2.023668362770559E-02
             8001     4.221377013554704E-02
```

4.2.3 1.94% Enriched UO_2, 4.00% Gd

The gadolinium burnable absorber pins use 1.944% enriched uranium with 4 wt% gadolinium. Since the density is not specified in the benchmark, it is assumed to be 10.24 g/cc as in the 2.46% enriched fuel and is consistent with a report produced by DeHart and Bowman (Reference 6).

VERA Input:

```
fuel GDU4  10.24 99.2 / 1.944 / gad=4.0
```

MPACT Echo:

```
+----------------------------------------+
| XS Record Name | Number Density (#/b-cm) |
+----------------------------------------+
           92234     3.542981540895427E-06
           92235     4.316293840282735E-04
           92236     1.977069384294944E-06
           92238     2.149108123254666E-02
            8001     4.385632402870474E-02
           64152     2.721913624083204E-06
           64154     2.966884886729854E-05
           64155     2.014217637747617E-04
           64156     2.785877067008526E-04
           64157     2.129900204241433E-04
           64158     3.380635661947831E-04
           64160     2.975063241654610E-04
            8016     2.042031154721232E-03
```

4.2.4 AIC

The silver-indium-cadmium (AIC) rods use the default AIC definition within VERA with 80% Ag, 15% In, and 5% Cd with a density of 10.146 g/cc based on the mass and volume of each rod specified in the benchmark. The AIC rods use 6063 aluminum cladding.

VERA Input:

```
mat AgInCd 10.146 aic
```

MPACT Echo:

```
+----------------------------------------+
| XS Record Name | Number Density (#/b-cm) |
+----------------------------------------+
           47107     2.349080557036007E-02
           47109     2.182423753330330E-02
           48000     2.717376506475383E-03
           49113     3.424401331820707E-04
           49115     7.639823360995234E-03
```

4.2.5 B_4C

The benchmark specification provides some description of the B_4C material, such as the material is compacted to 2.233 g/inch and the percentage of total boron and total carbon, but not a lot of detail on the boron enrichment. For this reason, the number densities used in similar Shift (Reference 14) inputs were used directly. In addition, the consistency in these data allows for future direct comparisons to be made between MPACT and Shift. Finally, the B_4C rods use 6061 aluminum cladding.

VERA Input:

```
mat b4c 1.281 B-10 1.4542912E-01
              B-11 6.4361958E-01
              C-00 2.1095335E-01
```

MPACT Echo:

```
+-----------------------------------------+
| XS Record Name | Number Density (#/b-cm) |
+-----------------------------------------+
             5010     1.120447643897759E-02
             5011     4.509928032839470E-02
             6000     1.017710963623270E-02
```

4.2.6 Stainless Steel

The standard VERA definition of stainless steel was used at 8.0 g/cc. It should be noted that the stainless steel used in the detector specification had a reduced density of 5.8 g/cc.

VERA Input:

```
mat ss 8.0
```

MPACT Echo:

```
+-----------------------------------------+
| XS Record Name | Number Density (#/b-cm) |
+-----------------------------------------+
             6000     3.211514299189242E-04
            24050     7.649141533953421E-04
            24052     1.475071567347299E-02
            24053     1.672598418229688E-03
            24054     4.163422096957057E-04
            26054     3.447775644607615E-03
            26056     5.412292264336241E-02
            26057     1.249930963613810E-03
            26058     1.663407737110646E-04
            25055     1.753869548455444E-03
            28058     5.308510941413849E-03
            28060     2.044841473936598E-03
            28061     8.888733282276648E-05
            28062     2.834149142606187E-04
            28064     7.217677666785675E-05
            15031     6.999302205390955E-05
            14000     1.715385996232905E-03
```

4.2.7 Inconel

Inconel is used as part of the detector specification at 8.43 g/cc. Again, the predefined VERA composition was used.

VERA Input:

```
mat inc 8.430
```

MPACT Echo:

```
+-----------------------------------------+
| XS Record Name | Number Density (#/b-cm) |
+-----------------------------------------+
            24050     6.363381551032824E-04
            24052     1.227123167753977E-02
            24053     1.391447425088600E-03
            24054     3.463584355545232E-04
            26054     3.719438323048593E-04
            26056     5.838745289494142E-03
            26057     1.348417307090418E-04
            26058     1.794473795112905E-05
            28058     4.298426612859908E-02
            28060     1.655755983399304E-02
            28061     7.197420097712686E-04
            28062     2.294877573174278E-03
            28064     5.844324066962681E-04
            14000     4.518969983826059E-03
            22000     2.650784117570579E-03
```

4.2.8 6061 Aluminum

Used in the 2.46% enriched UO_2 and B_4C rods, the composition of 6061 aluminum was used as described in a report by PNNL (Reference 4). This is almost identical to what is shown in the referenced report, but the manganese and titanium weight fractions have been slightly modified so the total sums to unity.

VERA Input:

```
mat alum61 2.70 Al-27 0.972
                Cr-00 0.00195
                Cu-63 0.00275
                Fe-00 0.0058
                Mg-00 0.01
                Mn-55 0.00075
                Si-00 0.006
                Ti-00 0.00075
```

MPACT Echo:

```
+-----------------------------------------+
| XS Record Name | Number Density (#/b-cm) |
+-----------------------------------------+
            13027     5.857469702346026E-02
            24000     6.097922307392727E-05
            29063     7.105463736977512E-05
            26000     1.688735036178968E-04
            12000     6.689864054457707E-04
            25055     2.219741147263921E-05
            14000     3.473656642371633E-04
            22000     2.547016767772443E-05
```

4.2.9 6063 Aluminum

Note that 6063 aluminum is not available in the PNNL report (as with 6061 aluminum), so the composition guideline from Aerospace Specification Metals, Inc. (ASM) was used to determine the composition (Reference 7).

VERA Input:

```
mat alum63 2.70 Al-27 0.978
                Cr-00 0.001
                Cu-63 0.001
                Fe-00 0.0035
                Mg-00 0.009
                Mn-55 0.00075
                Si-00 0.006
                Ti-00 0.00075
```

MPACT Echo:

```
+-----------------------------------------+
| XS Record Name | Number Density (#/b-cm) |
+-----------------------------------------+
           13027     5.893626922730878E-02
           24000     3.127139644816783E-05
           29063     2.583804995264550E-05
           26000     1.019064245970067E-04
           12000     6.020877649011937E-04
           25055     2.219741147263921E-05
           14000     3.473656642371633E-04
           22000     2.547016767772443E-05
```

4.2.10 Rhodium

A small amount of rhodium was used in the detector model. This was assumed to be completely Rh-103 at 12.41 g/cc.

VERA Input:

```
mat rh103 12.41 Rh-103 1.0
```

MPACT Echo:

```
+-----------------------------------------+
| XS Record Name | Number Density (#/b-cm) |
+-----------------------------------------+
           45103     7.262501667450562E-02
```

4.2.10 Borated Moderator

The borated moderator also used some of the VERA input capability, where a 0.997048 g/cc density was specified and the soluble boron concentration (ppm) was input. The values below were for Core 8:1.

VERA Input:

```
modden 0.997048  ! [g/cc] water at STP
boron  1337.9    ! ppm
```

MPACT Echo:

```
+-----------------------------------------+
| XS Record Name | Number Density (#/b-cm) |
+-----------------------------------------+
             1001     6.660332543317464E-02
             8016     3.330166271658732E-02
             5010     1.478690256725317E-05
             5011     5.951914048427026E-05
```

4.3 Results

Table 9 shows the results for the various core configurations. As all configurations should be critical, the difference reported is just the eigenvalue difference from unity. In general, there is a clear bias in the TCP_0 results, which tend to be 150-200 pcm low. A similar trend is observed with P_2 scattering, where Cores 8:1 – 8:10 have roughly a -100 pcm bias, though the eigenvalue for Cores 8:12 – 8:17 tend to be a bit higher than critical. The standard deviation, root mean square, and maximum errors are summarized as well.

Table 9. B&W-1810 Benchmark Results

Core	Short Description	TCP0		P2	
		Eig.	Diff. (pcm)	Eig.	Diff. (pcm)
1	0 Gd	0.99809	-191	0.99981	-19
2	0 Gd, AIC Rods	0.99757	-243	0.99915	-85
3	20 Gd	0.99778	-222	0.99933	-67
4	20 Gd, AIC Rods	0.99840	-160	0.99990	-10
5	28 Gd	0.99749	-251	0.99899	-101
5A	32 Gd	0.99739	-261	0.99888	-112
5B	28 Gd	0.99755	-245	0.99905	-95
6	28 Gd, AIC Rods	0.99770	-230	0.99918	-82
6A	32 Gd, AIC Rods	0.99765	-235	0.99912	-88
7	28 Gd (annular)	0.99749	-251	0.99899	-101
8	36 Gd	0.99762	-238	0.99910	-90
9	36 Gd, AIC Rods	0.99752	-248	0.99900	-100
10	36 Gd, Void Rods	0.99743	-257	0.99889	-111
12	0 Gd	0.99886	-114	1.00092	92
13	0 Gd, B4C Rods	0.99901	-99	1.00056	56
14	28 Gd	0.99854	-146	1.00024	24
15	28 Gd, B4C Rods	0.99887	-113	1.00030	30
16	36 Gd	0.99851	-149	1.00015	15
17	36 Gd, B4C Rods	0.99848	-152	0.99990	-10
Cores 1-10	2.46% Enriched Throughout	STDDEV	29	STDDEV	32
		RMS	235	RMS	87
		MAX	261	MAX	112
Cores 12-17	4.02% Enriched Inner Core, 2.46% Outer	STDDEV	23	STDDEV	35
		RMS	131	RMS	47
		MAX	152	MAX	92
Total		STDDEV	56	STDDEV	64
		RMS	208	RMS	77
		MAX	261	MAX	112

Figures 11-14 show the difference in the midplane fission rate distributions. In the figures for Cores 8:5 and 8:14, the burnable absorber pins are highlighted with a purple boundary. In general, the results look good, but there is still room for improvement, particularly in Core 8:12 and 8:14, which have the 4.02% fuel in this assembly, where the errors are notably higher.

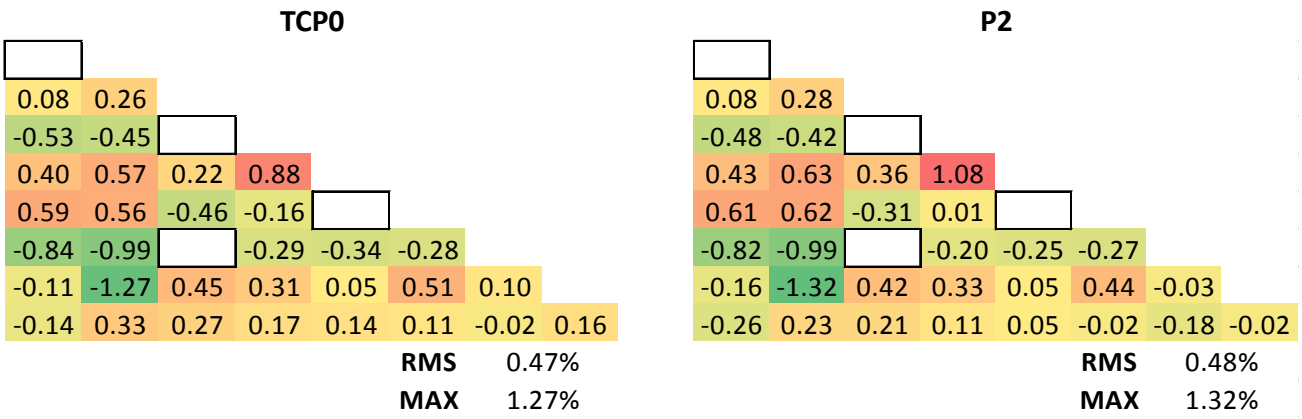

Figure 11: B&W-1810 Core 8:1 Fission Rate Difference, Center Assembly

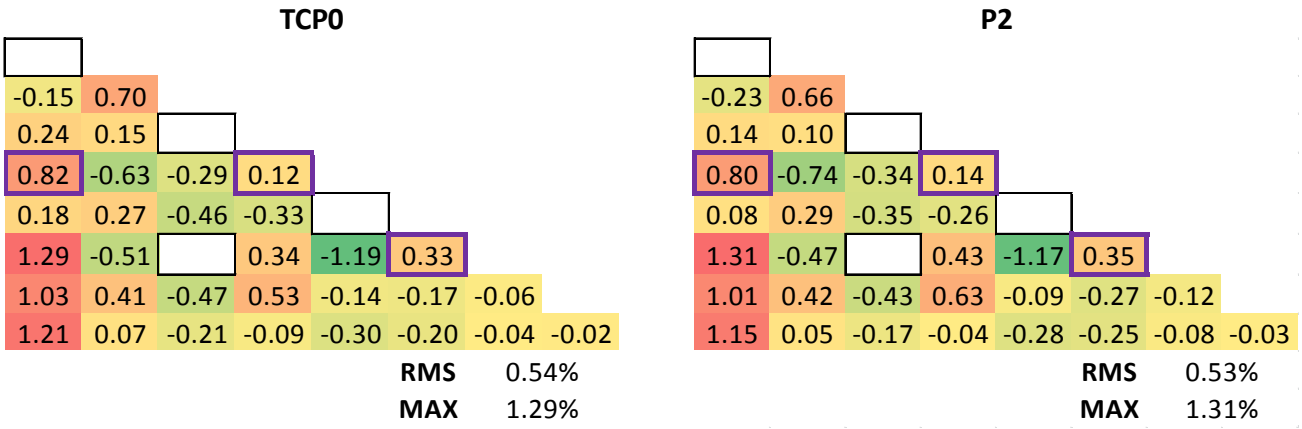

Figure 12: B&W-1810 Core 8:5 Fission Rate Difference, Center Assembly

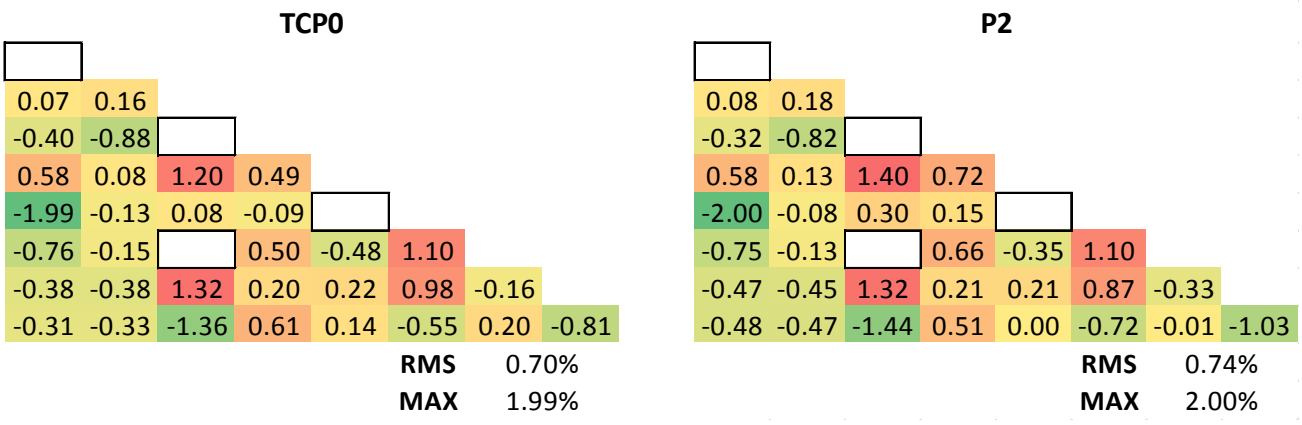

Figure 13: B&W-1810 Core 8:12 Fission Rate Difference, Center Assembly

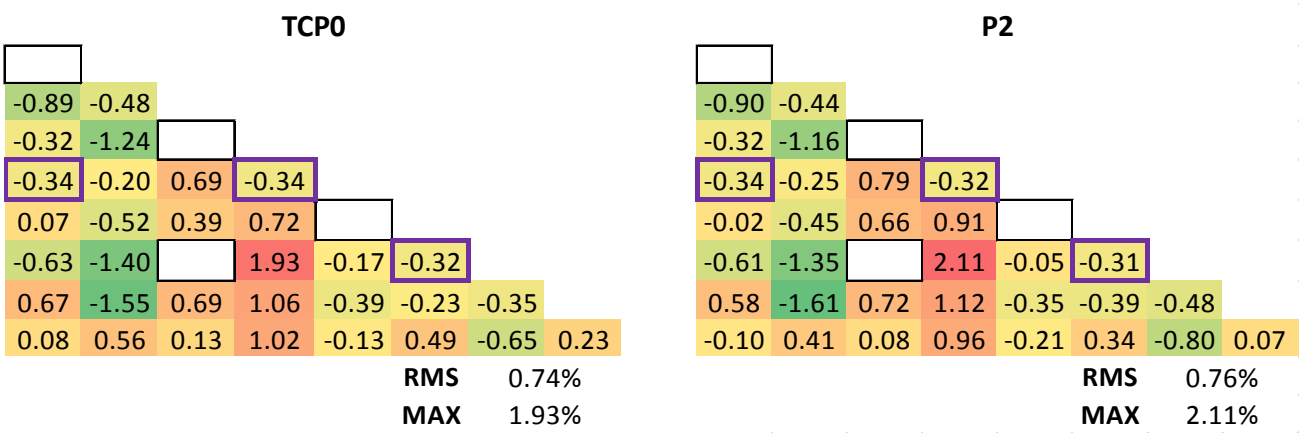

Figure 14: B&W-1810 Core 8:14 Fission Rate Difference, Center Assembly

Many comparable results are available for both eigenvalue and the fission rate distributions (References 8-11). However, there are some noteworthy differences. For example, References 8 and 9 used a buckling value of 3.7×10^{-4} cm^{-2}, whereas the work performed in CASMO (Reference 10) used the same 4.1×10^{-4} cm^{-2} used in this work. It is unclear exactly what value Reference 11 used.

In comparing to the results from TransLAT (Reference 8), the eigenvalues from MPACT are notably worse as TransLAT yields an RMS of 56 pcm and a MAX of 128 pcm. However, comparison of the fission rates shows that the MPACT distributions are significantly better, particularly for Cores 1 and 5.

Reference 9 reports only the eigenvalue, which tend to be roughly 175 pcm higher than critical, but this was with ENDF/B-VI.8 cross section data and with a lower buckling value. ENDF/B-VII results are included but seem to be very preliminary as the average is over 700 pcm off.

The results from CASMO (Reference 10) show excellent agreement in eigenvalue with an average of -47 pcm for Cores 8:1 – 8:17. An enrichment bias with the higher enriched inner cores is also not present and similar results are observed for all cores. Unfortunately, no fission rate distribution comparisons are available from this reference.

Lastly, a paper on the AEGIS code (Reference 11) reports only results for Cores 8:1 and 8:5 with eigenvalues of 1.00152 and 1.00057, which are notably better than the MPACT results with TCP_0 scattering. In the fission rate distribution comparisons, the AEGIS paper reported a relative difference compared to the experiment. In this case, the MPACT results for Core 8:1 are very similar, with a slight improvement in the RMS. However, for Core 8:5, the maximum errors from MPACT are significantly larger (~4.75% vs 2.14%) because of the lower power burnable absorber pins, though the RMS is only marginally worse (1.03% vs 0.86%).

So while the MPACT results are certainly very reasonable, there is room for improvement. Much of this improvement could likely come from the cross section library, particularly in the accuracy of the transport correction.

Finally, Figure 15 shows the fission rate differences along the diagonal pins for Cores 8:5 and 8:14. Again, the locations with the burnable absorber pins are highlighted in purple. This data is normalized in a similar manner to the center assembly comparisons, where only the center assembly fission rate normalizes to unity. A clear bias is observed, particular near the periphery where almost all of the fission rates are underpredicted.

Core 5

Pin Index	MEAS	Diff. (%) TCP0	Diff. (%) P2
0	0.000	---	---
1	0.999	0.70	0.67
2	0.000	---	---
3	0.181	0.12	0.16
4	0.000	---	---
5	0.187	0.33	0.37
6	1.018	-0.06	-0.10
7	1.070	-0.02	-0.03
8	1.067	0.08	0.10
9	1.018	-0.62	-0.58
10	0.187	0.15	0.21
11	0.000	---	---
12	0.177	0.21	0.30
13	0.000	---	---
14	1.028	-1.80	-1.43
15	0.000	---	---
16	1.016	-0.55	-0.17
17	0.000	---	---
18	0.961	0.23	0.76
19	0.000	---	---
20	0.799	1.13	1.54
21	0.728	-1.56	-1.28
22	0.641	0.35	0.58
23	0.590	-1.30	-1.11
24	0.527	-2.10	-1.95
25	0.439	-0.62	-0.54
26	0.366	-0.63	-0.64
27	0.293	-0.27	-0.35
28	0.236	-0.60	-0.70
29	0.193	-0.50	-0.56
30	0.188	-0.62	-0.61

Core 14

Pin Index	MEAS	Diff. (%) TCP0	Diff. (%) P2
0	0.000	---	---
1	1.080	-0.48	-0.33
2	0.000	---	---
3	0.164	-0.34	-0.29
4	0.000	---	---
5	0.162	-0.32	-0.28
6	0.965	-0.35	-0.38
7	0.959	0.23	0.16
8	0.917	0.66	0.59
9	0.864	-1.08	-1.13
10	0.133	-0.36	-0.34
11	0.000	---	---
12	0.113	-0.31	-0.28
13	0.000	---	---
14	0.663	-1.31	-1.30
15	0.000	---	---
16	0.470	-3.02	-3.01
17	0.000	---	---
18	0.394	-1.63	-1.61
19	0.000	---	---
20	0.303	-1.05	-1.08
21	0.273	-2.40	-2.47
22	0.238	-1.95	-2.03
23	0.201	-1.07	-1.15
24	0.174	-1.11	-1.19
25	0.145	-0.86	-0.94
26	0.119	-0.78	-0.87
27	0.094	-0.59	-0.69
28	0.073	-0.47	-0.55
29	0.059	-0.50	-0.56
30	0.055	-0.53	-0.58

Figure 15: B&W-1810 Core 8:5 and 8:14 Fission Rate Difference, Diagonal Pins

5. REFERENCES

1. M. N. Baldwin and G. S. Hoovler, "Critical Experiments Supporting Close Proximity Water Storage of Power Reactor Fuel," Tech. Rep. BAW-1484-1, The Babcock & Wilcox Company, 1978.
2. L. W. Newman, W. A. Wittkopf, W. G. Pettus, M. N. Baldwin, H. A. Hassan, V. O. Uotinen, J. D. Connell, and P. S. Campbell, "Urania Gadolinia: Nuclear Model Development and Critical Experiment Benchmark," Tech. Rep. BAW-1810, The Babcock & Wilcox Company, 1984.
3. J. K. Tuli, Nuclear Wallet Cards. National Nuclear Data Center, Brookhaven National Laboratory, Upton, NY, USA, eighth ed., 2011.
4. R. J. McConn Jr., C. J. Gesh, R. T. Pagh, R. A. Rucker, and R. G. Williams III, "Compendium of Material Com- position Data for Radiation Transport Modeling," Tech. Rep. PNNL-15870, Rev. 1, Pacific Northwest National Laboratory, 2011.
5. C. A. Wemple, "Benchmarking the HELIOS-2 ENDF/B-VII Library: B&W-1484 and DIMPLE S-06 Criticals," in Proceedings of Advances in Nuclear Fuel Management IV (ANFM 2009) Topical Meeting, (LaGrange Park, IL, USA), American Nuclear Society, 2009.
6. M. D. DeHart and S. M. Bowman, "Analysis of Fresh Fuel Critical Experiments Appropriate for Burnup Credit Validation," ORNL/TM-12959, Oak Ridge National Laboratory, October, 1995.
7. ASM Aerospace Specification Metals, Inc, "Aluminum 6063-T6," Access Online: http://asm.matweb.com/search/SpecificMaterial.asp?bassnum=MA6063T6, April, 2015.
8. S. P. Baker, "TransLAT Lattice Physics Code Benchmark to B&W Gadolinia Criticals," *Proc. of PHYSOR 2004*, Chicago, IL, 2004.
9. K. H. Lee, et al., "KARMA 1.1 Benchmark Calculations for the B&W Critical Experiments with ENF/B-VI R8 and ENDF/B-VII R0", *Proc. Kor. Nucl. Soc.*, pg. 87-88, May 27-28, 2010.
10. J. Rhodes, et al. "CASMO-5 ENF/B-VII R0 Comparison to B&W Criticals Series 1810," *Proc. Am. Nucl. Soc.*, Vol. 97, pg. 577-579, November 11-15, 2007.
11. A. Yamamoto, et al., "AEGIS: An Advanced Lattice Physics Code for Light Water Reactor Analyses," *Nuclear Science and Technology*, Vol. 42, No. 5, October 2010.
12. International Criticality Safety Benchmark Evaluation Project (ICSBEP) Handbook, 2014 Edition, Nuclear Energy Agency & Idaho National Laboratory, 2014.
13. S. M. Bowman, "SCALE 6: Comprehensive Nuclear Safety Analysis Code System," *Nucl. Tech.* 174(2), 126-148, 2011.
14. T. Evans et al., "Exnihilo Documentation: Release 5.1 (Dev)," Oak Ridge National Laboratory, August 2014.
15. B. R. Herman, B. Forget, and K. Smith, "Improved Diffusion Coefficients Generated from Monte Carlo Codes," in *Proceedings of the M&C 2013 ANS Meeting*, (LaGrange Park, IL, USA), American Nuclear Society, 2009.

APPENDIX A: B&W-1484 KENO EXECUTIONS

In order to act as an additional form of verification for MPACT as well as to provide future analysts with updated models, Core 4:1 and 4:2 were retrieved from the ICSBEP handbook (Reference 12) and updated to function with a modern version of KENO (in this case, KENO V.a). From the ICSBEP, Cores 4:1 and 4:2 correspond to the inputs named LCT01101 and LCT01102 from LEU-COMP-THERM-011, respectively.

In addition to running the traditional 3D case, 2D cases were run with materials that represented the core midplane elevation to provide a direct comparison to the unbuckled MPACT runs. In addition, the 2D and 3D KENO models are compared to directly quantify the effect of axial leakage that the buckling attempts to emulate. Plan and elevation views of the Core 4:1 and 4:2 models are shown in Figures 16 & 17 and 18 & 19, respectively.

The eigenvalues calculated in each of the KENO executions are summarized in Table 10.

Table 10. B&W-1484 KENO-Calculated 2D & 3D Eigenvalues

	Core 4:1 k_{eff}	Core 4:2 k_{eff}
KENO, 3D	0.99909±0.00039	1.00045±0.00037
KENO, 2D	1.01324±0.00035	1.01494±0.00039
KENO, 3D/2D	0.98603	0.98572

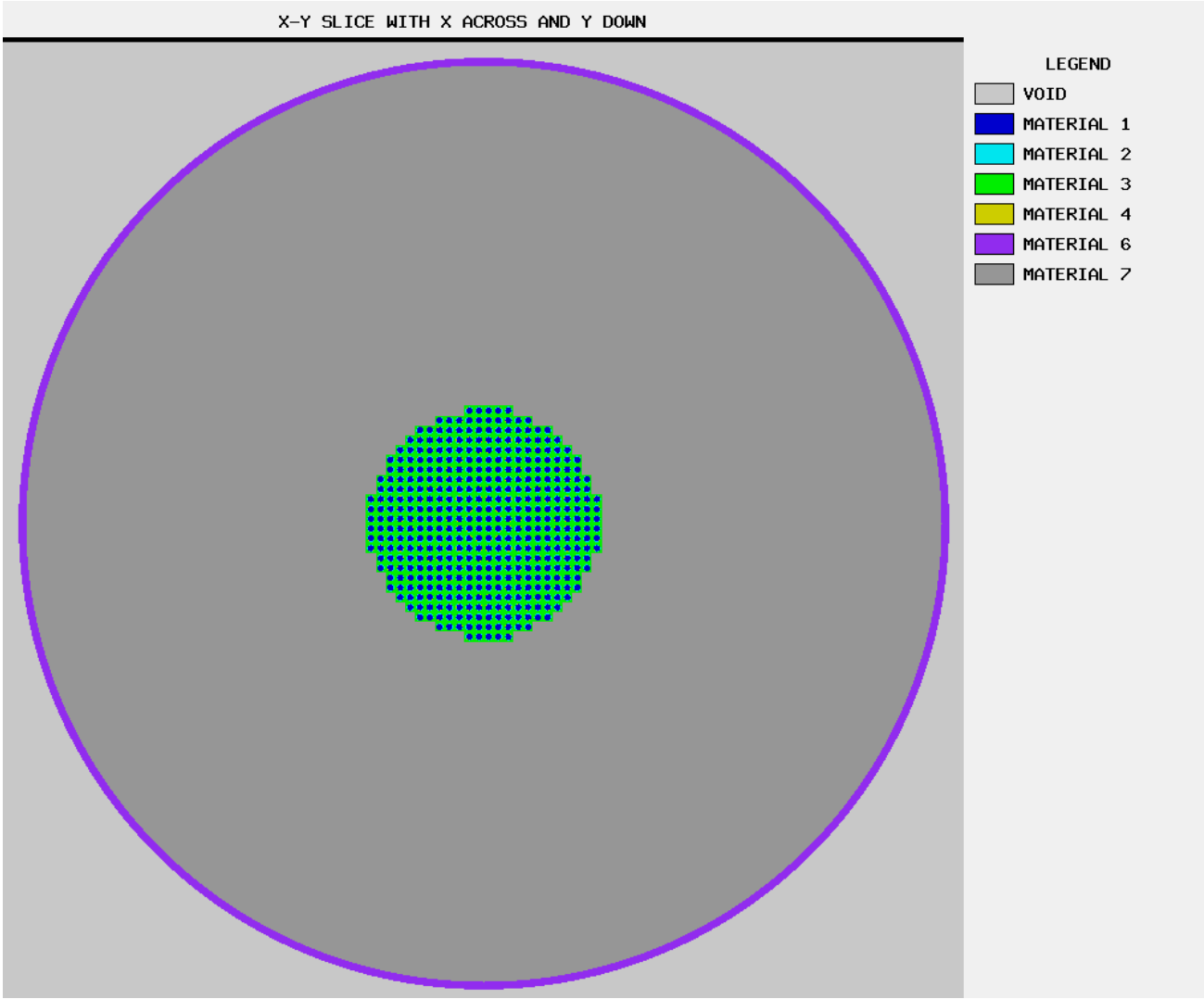

Figure 16: B&W-1484 Core 4:1 KENO Model Plan View

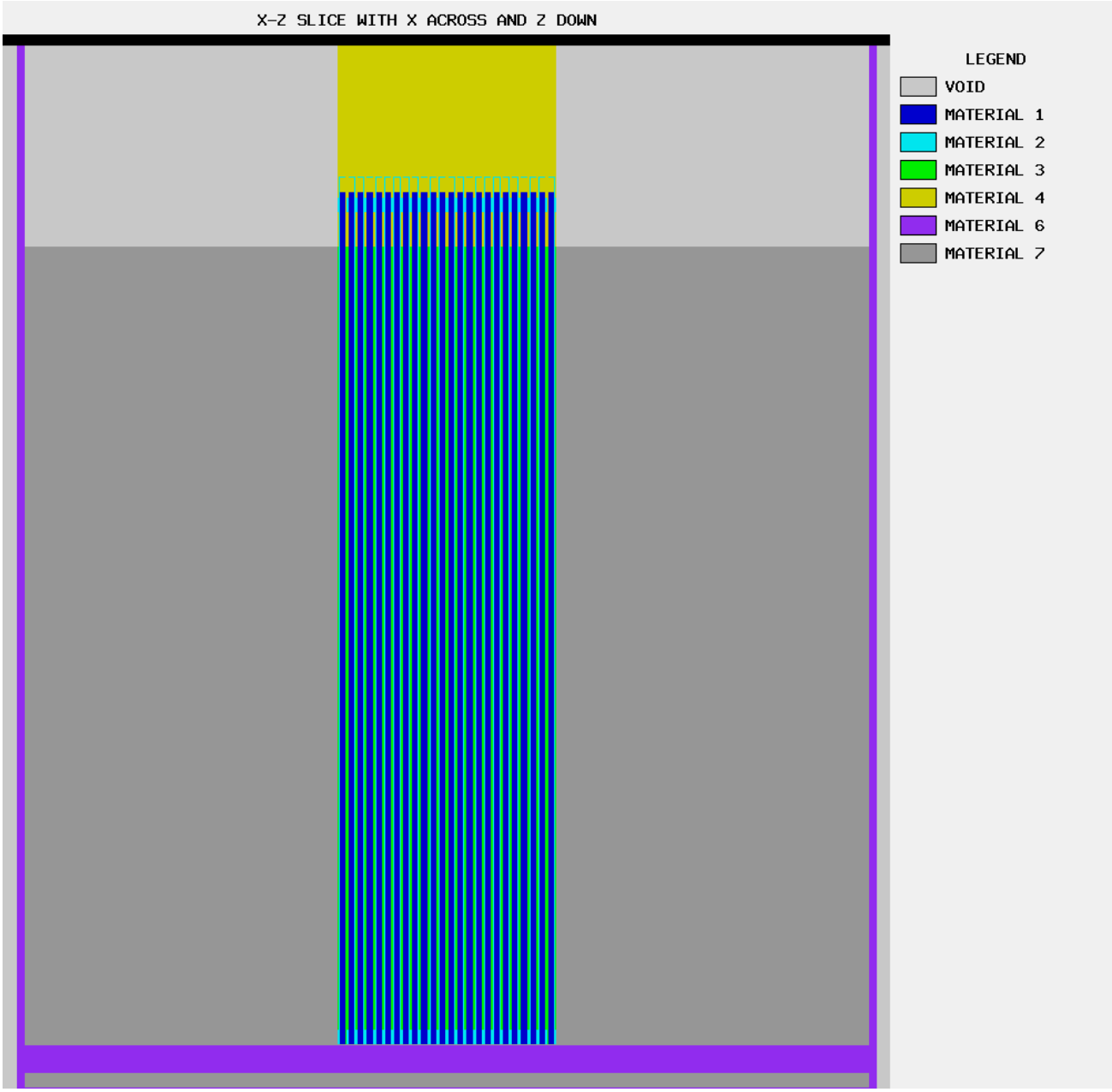

Figure 17: B&W-1484 Core 4:1 KENO Model Elevation View

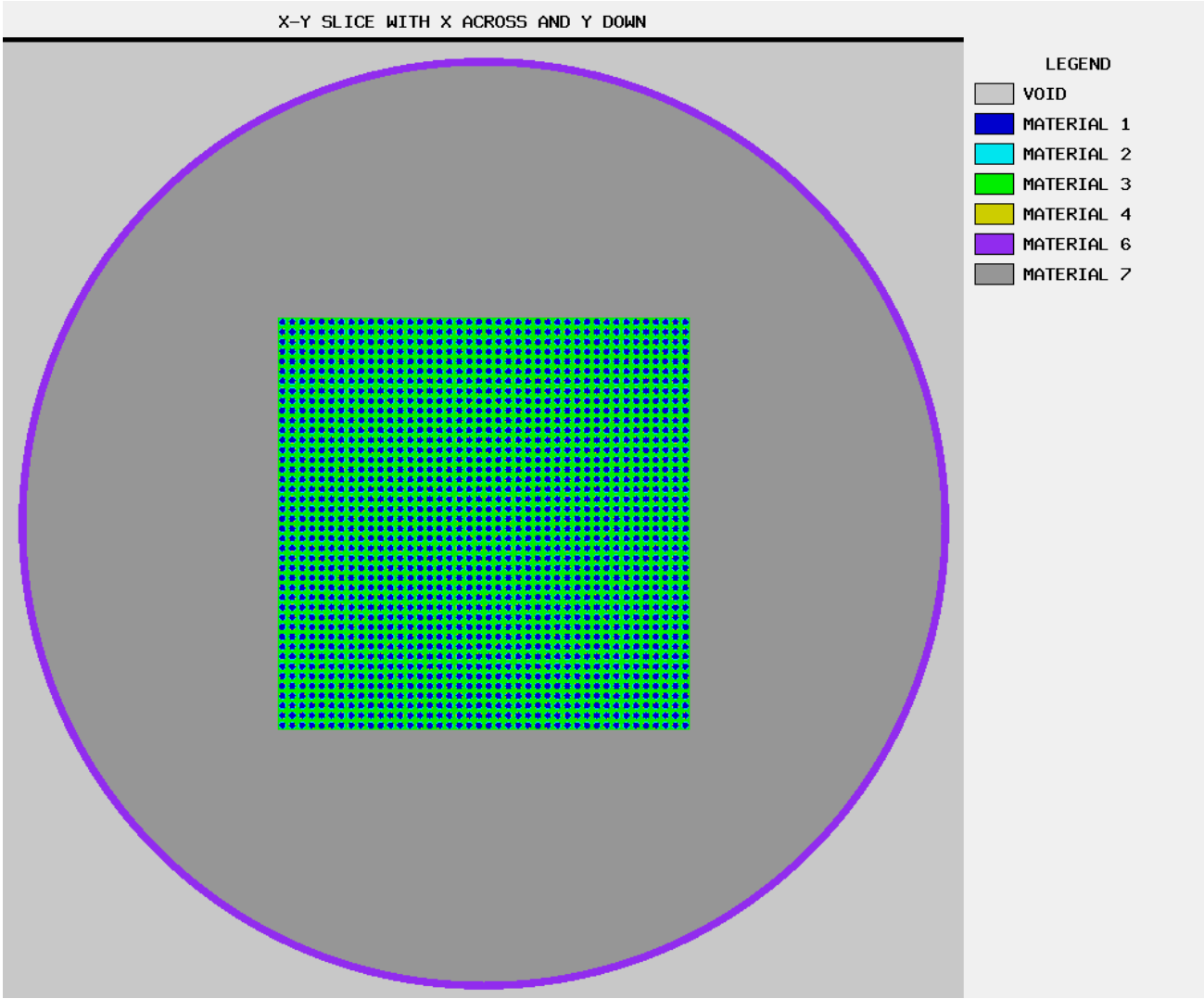

Figure 18: B&W-1484 Core 4:2 KENO Model Plan View

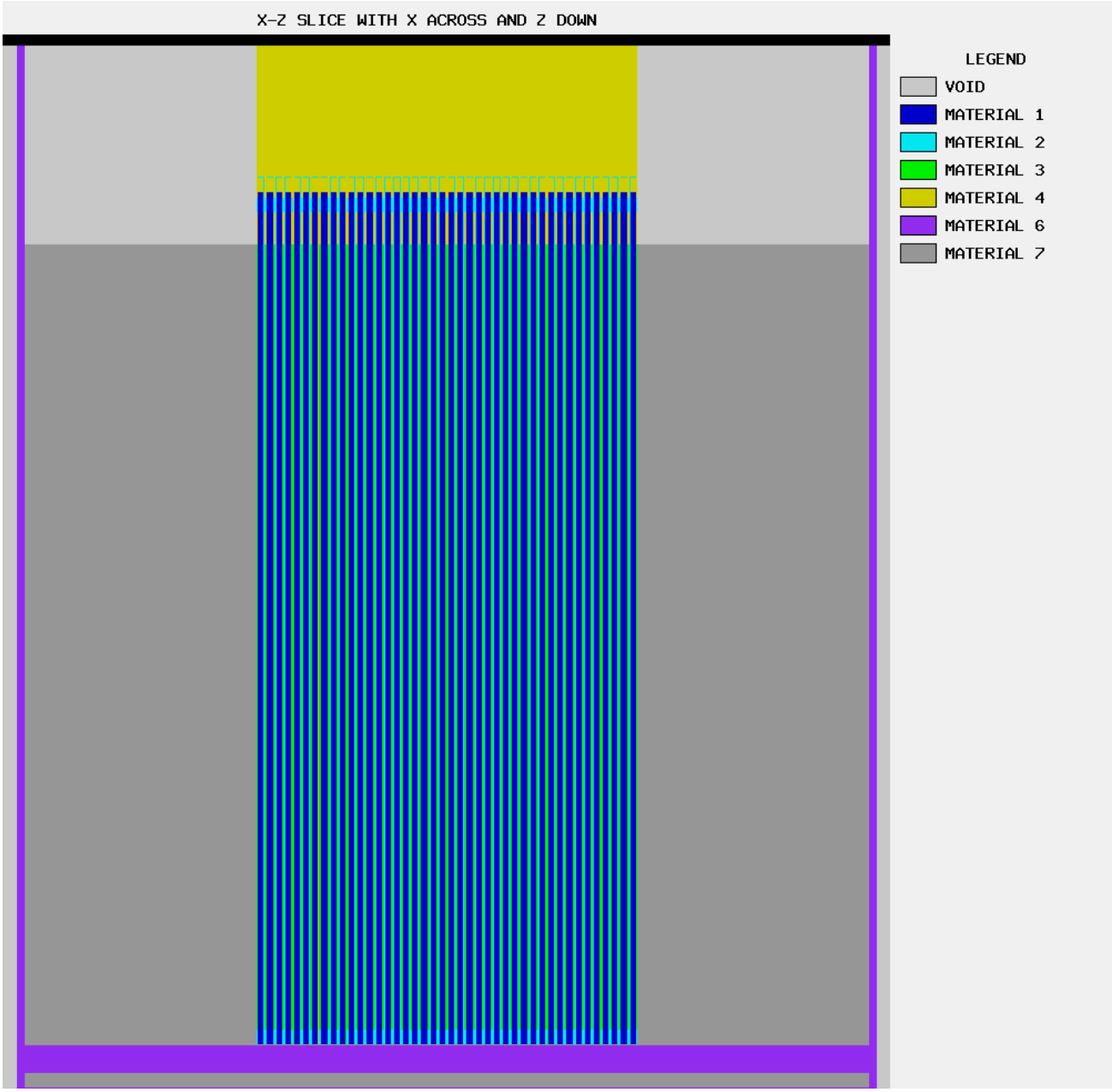

Figure 19: B&W-1484 Core 4:2 KENO Model Elevation View

APPENDIX B: B&W-1484 CORES 4:1 AND 4:2 BUCKLING SENSITIVITIES

This appendix describes the results of a sensitivity study run on the effect of varying buckling values for various scattering methods for both Cores 4:1 and 4:2. The purpose of this study was to assess the impact of the buckling, which directly drives neutron leakage, on the final value calculated for k_{eff} in these various cases. Figure 20 summarizes all cases executed while Figures 21 and 22, show results for Cores 4:1 and 4:2, respectively, as a function of specified buckling and corresponding extrapolation distance.

These results suggest that eigenvalue variation with buckling is both linear and weak, so the results are not strongly dependent on the buckling value selected.

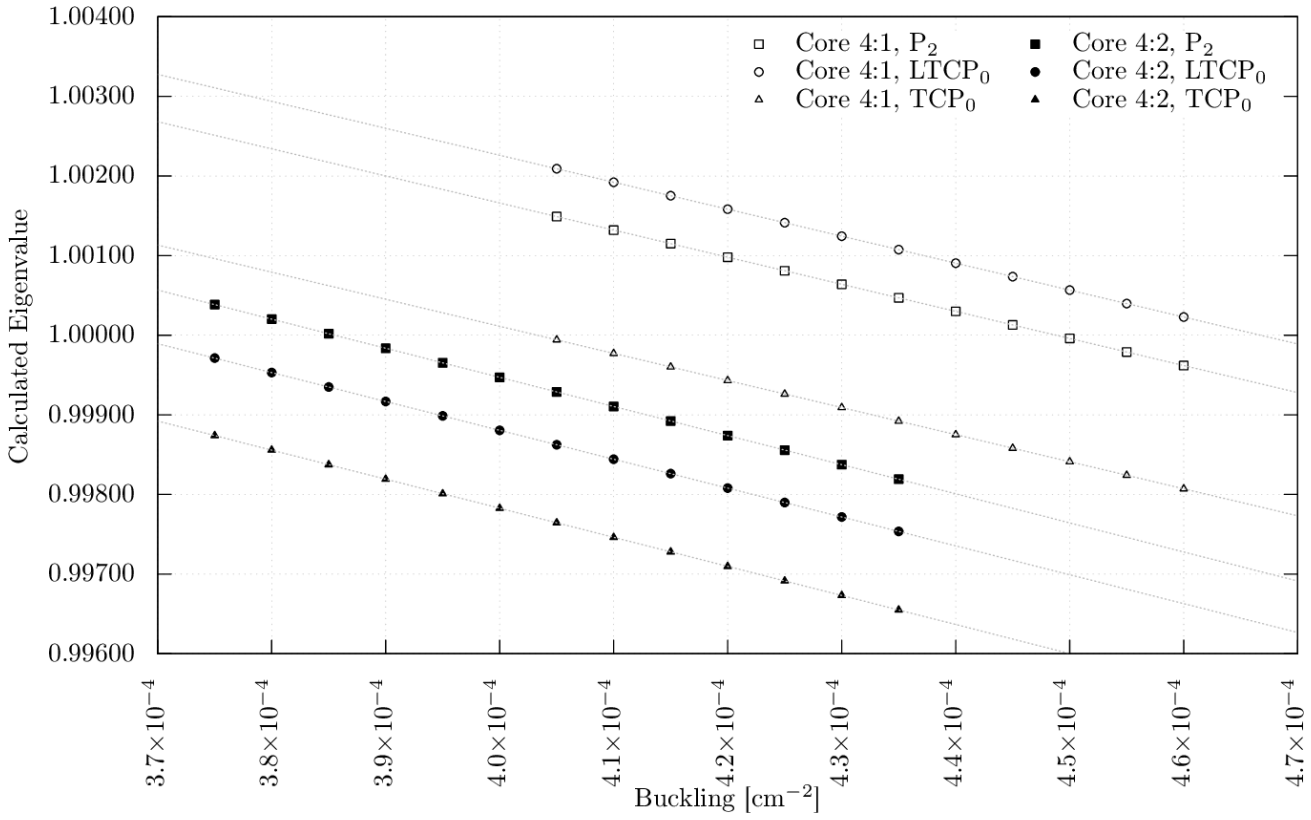

Figure 20: B&W-1484 Core 4:1 and 4:2 Buckling Sensitivity Results

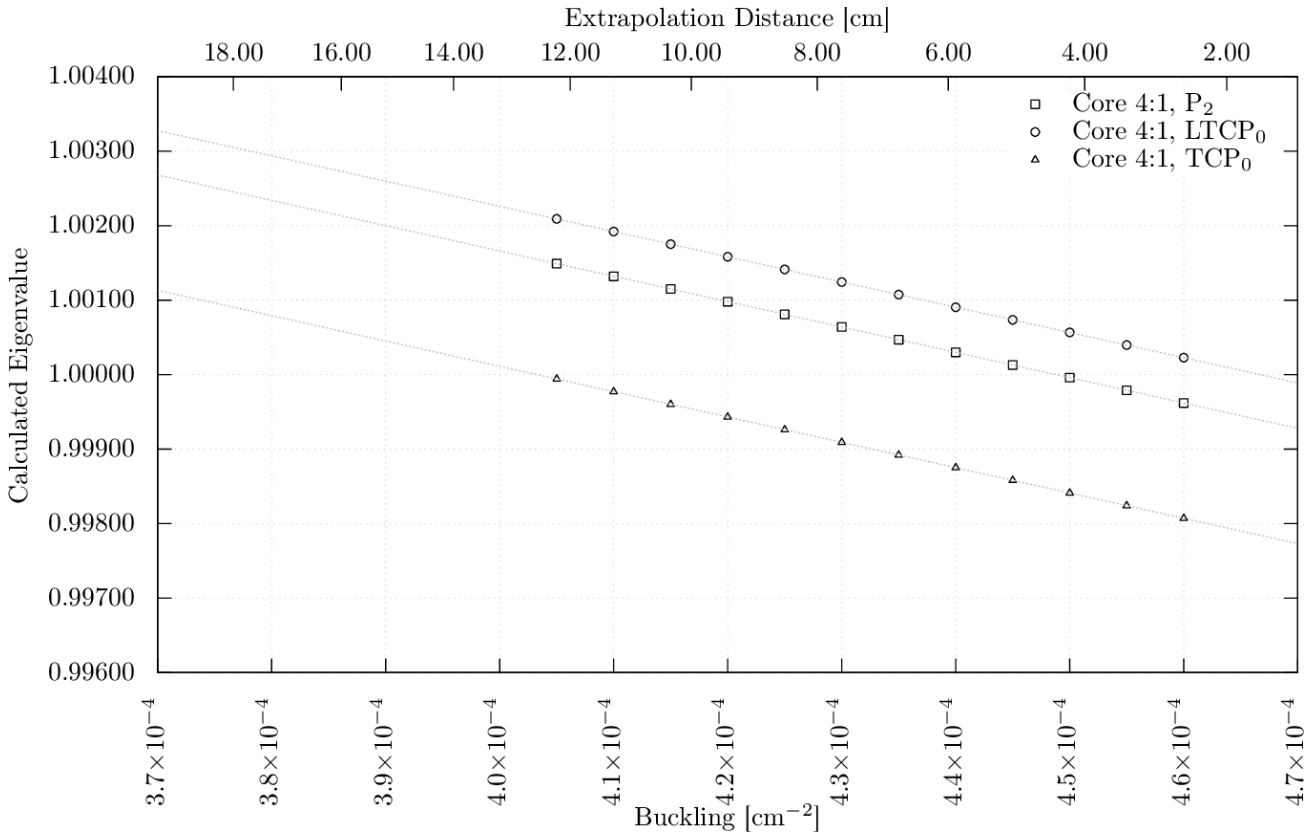

Figure 21: B&W-1484 Core 4:1 Buckling Sensitivity Results

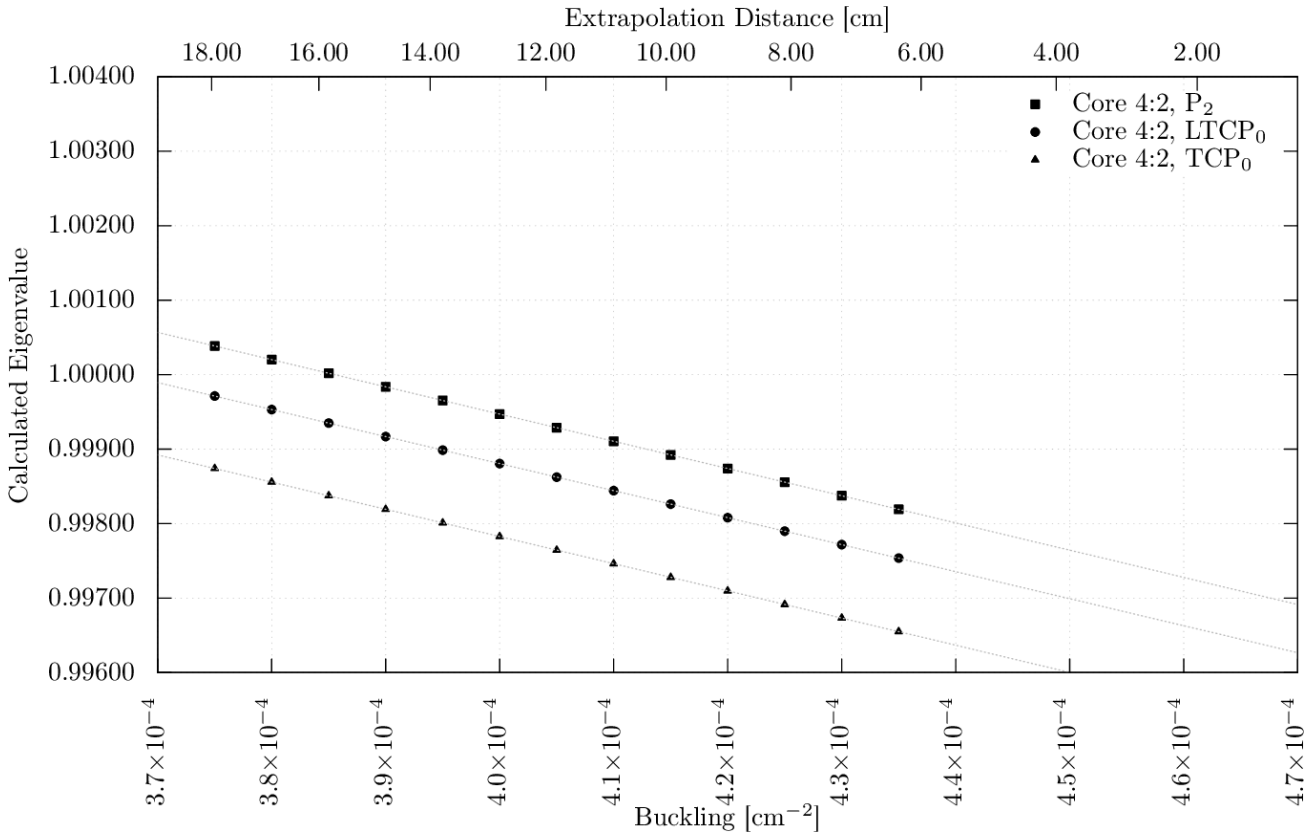

Figure 22: B&W-1484 B&W-1484 Core 4:2 Buckling Sensitivity Results